Aapg Bulletin
September 2016, Volume 100 Issue 9 Pages 1419-1442
http://dx.doi.org/10.1306/03101614087
http://archimer.ifremer.fr/doc/00352/46328/

Three-dimensional evolution of salt-controlled minibasins: Interactions, folding, and megaflap development

Callot Jean-Paul [1, *], Salel Jean-Francois [2, *], Letouzey Jean [3, *], Daniel Jean-Marc [4, *], Ringenbach Jean-Claude [5, *]

[1] Univ Pau & Pays Adour, Ave Univ, F-64013 Pau, France.
[2] Total E&P USA, 1201 Louisiana St,Suite 1800, Houston, TX 77002 USA.
[3] Univ Paris 06, Univ Paris 04, Inst Sci Terre Paris iSTeP, 4 Pl Jussieu, F-75005 Paris, France.
[4] IFREMER, F-29280 Plouzane, France.
[5] Total SA, Ctr Sci & Tech Jean Feger, Ave Larribau, F-64000 Pau, France.

* Corresponding authors email addresses : jean-paul.callot@univ-pau.fr ; jean-francois.salel@total.com ; jean.letouzey@wanadoo.fr ; jean-marc.daniel@ifpen.fr ; jean-claude.ringenbach@total.com ;

Abstract :

A megaflap, or an overturned, folded, sedimentary-basin edge, is a classic feature of salt-controlled basins, formed during the inception of salt allochthony. To illustrate the relative importance of the balance between salt and sediment inputs, basin rheology, and tectonism resulting from basin interactions in the development of megaflaps, a set of analog experiments were performed in a computed tomography scanner. Sediments are modeled using both granular material and a mix of granular and viscous material and salt as purely viscous material. Uneven sedimentary loading and associated salt flow localize primary minibasins, which then migrate and expand laterally until sufficient thickness is reached to pin the downbuilding phase. The encasement of minibasins into the mother-salt layer is followed by secondary minibasin development above the canopy, the inception and localization of which appear to be more locally controlled by the primary salt feeders, salt glaciers, and canopies. Enhanced salt extrusion along basin edges is responsible for (1) classic halokinetic sequences, (2) major wedging and basin-edge erosion, and (3) basin-edge backfolding onto the basin centers, forming megaflaps. Basin interactions during differential subsidence and secondary minibasin development above the allochthonous salt canopy result in the formation of salt welds and tectonic deformation at basin boundaries, including broken and transported basin edges. The major controlling factor in megaflap development is salt allochthony, which allows the local salt extrusion rate to be higher than the sedimentation rate. Enhanced allochthony is the result of enhanced pressure related to local salt stock squeezing, regional shortening, or basin tilting.

Introduction

Salt tectonics (i.e. evaporite controlled deformation) is a widely studied structural domain, but despite improved seismic imaging methods, the interpretation of evaporite related structures remains a challenge for both academic institutions and oil industry, due to the non-cylindrical geometries of syntectonic sediment, deposited during evaporite movement, and highly complex, sometimes vertical or overturned structural objects (e.g. Hudec and Jackson, 2006; 2009). Salt tectonics rely first on the inherent mechanical properties of salt rocks in general, which under geologic timescales behave as viscous fluids (e.g. Weijermars et al., 1993); and second, on the very low compressibility and low density of salt rocks, that makes them lighter than most of the compacted clastic and carbonates rocks (e.g. Hudec and Jackson, 2009; Hudec et al., 2009). Salt mobility is triggered and evolves along with few major processes, namely gravitational spreading under differential loading, and gravitational gliding along a slope (e.g. Hudec and Jackson, 2007; Rouby et al., 2002; Fort and Brun 2012, Rowan et al., 2013), shortening (Rowan and Vendeville, 2006; Callot et al., 2007; 2012) and basement tectonics (Coward and Stewart, 1995). Salt may also flow at surface as glacier under its own weight (Such as in Iran, Talbot 1998). Tectonically and topographically controlled pressures, salt hydration degree, as well as thermal gradient, modify the equilibrium of salt masses relatively to the overburden. Buoyancy alone, for a long time considered as the main driving force is now considered to be of lesser importance than lateral pressure gradients related to differential loading processes or regional tectonic (e.g. Hudec and Jackson, 2007; Rowan et al. 2013 and discussion therein).

The main tectonic styles of evaporitic basins have been described during the last decades in the framework of (1) passive margins suffering sediment gliding above an evaporite décollement (such as in the Gulf of Mexico, or Angolan and Brazilian margins, e.g. Burrollet, 1975 ; Spathopouolos 1996; Fort et al., 2004), in which thick salt basin receiving high amount of sediments may develop gravitational spreading; (2) intracratonic or rifted basins where salt motion is mostly vertical with a dual tectonic and sedimentary control of the evaporite motion (German Zechstein basins, e.g. Mohr et al., 2006 and Pricaspian basin in Kazakhstan, e.g. Volozh et al., 2003); (3) Pre-existing salt provinces and structures triggered by shortening (such as the Zagros (Iran) or Kuche (Tarim Basin China) fold and thrust belts, e.g. Vendeville and Rowan, 2006; Callot et al., 2012), or inverted during compression (e.g. North Sea, Coward and Stewart 1995).

These salt tectonic provinces are characterized by the emplacement of salt wall, diapirs, rim synclines, overhangs, which record the evolution of major depocentres during salt withdrawal (e.g. Jackson et al., 1986; Rowan et al., 2003; Mohr et al., 2006), and in the case of gravitational gliding, to rollover, turtle-back anticlines, and toe-thrust systems at salt distal pinch out (e.g. Fort et al. 2004). A key point is the ubiquity of minibasin development in any setting, as soon as the initial salt thickness is high enough to allow for massive downbuilding and evaporite.

The case of very thick salt basin, associated to large amount of sedimentation, such as the Gulf of Mexico, has been a particular topic of interest on its own, due to intense exploration activity and search for hidden traps. The Gulf of Mexico, as well as the central part of the Angolan margin salt basin, are particularly characterized by isolated minibasins and salt canopies (e.g. Rowan, 1995; Fort and Brun, 2004; Hudec and Jackson, 2006; 2009, and reference therein; Ringenbach et al., 2013). Such structures are favoured by the initial high thickness of the salt layer, enabling rapid salt flow and vertical accommodation space creation, and a high sediment influx (Diegel et al., 1995; Pilcher et al., 2011; Fort and Brun, 2012). In the central Gulf of Mexico, secondary minibasins occurring on the successive canopies are well imaged on seismic. But despite new seismic acquisition methods such as WATS (Wide Azimut Towed-Streamer Seismics), imaging the primary minibasins below the thick canopy remains a challenge, as the geometries are poorly retrieved along the salt structures. Their interpretation relies thus both on well data and comparison with laboratory scaled models (e.g. Rowan and Vendeville, 2006; Dooley et al., 2012) as well as field analogue, which are a few (Giles and Lawton, 2002; Harrison and Jackson, 2006; 2012; Rowan and Vendeville, 2006; Hearon 2012; Ringenbach et al., 2013; Callot et al., 2014). Besides these classical cases, minibasins also occur in the other systems listed above, provided salt was thick and that at a stage, abundant sedimentation was the main driver.

Among the most impressive structures associated to salt tectonics, the megaflaps have been recently recognized, both in seismic and in well-known outcrop analogues (see Davison et al., 1996; Graham et al., 2012; Ringenbach et al., 2013; Callot et al., 2014; Alsop et al., 2015; Hearon et al., 2015). The mechanisms responsible for their development, the geometrical relationship with adjacent undeformed sediments confining the flap, as well as the structural style associated to such structures remain poorly constrained. The present paper thus describes a set of analogue experiments performed in order to reproduce the geometries and kinematic evolution of minibasins controlled by sedimentation only developed ontop of a thick ductile layer, with the particular aim to reproduce megaflaps. Experiment were

performed at IFP-EN (Rueil-Malmaison, France) using a medical scanner (e.g. Colletta et al., 1991; Callot et al., 2012) to image minibasins evolution in 3D and through time without mechanical interference with the model during the course of the experiments. The geometries and kinematic evolution of both single and populations of minibasins imaged in 3D are then compared to seismic and field examples.

Minibasin paradigm and previous works

Minibasins

The term minibasin (figure 1) was introduced by Worall and Snelson (1989), following early decription of sedimentary basins controlled by salt withdrawal (see Trusheim, 1960, and Lehner, 1969). Such sedimentary accumulation related to salt escape was defined as "a synkinematic basin subsiding into relatively thick, allochthonous or autochthonous salt" independently from the basement absolute subsidence (pp16, Jackson and Talbot, 1991), a definition which is mostly descriptive and should not bear any *a priori* mechanical assumption. From then on, such sedimentary basins have been widely described in various settings: above the Aptian salt of the Brazilian and Angolan margins (e.g. Cobbold et al., 1995; Hudec and Jackson, 2004); in the Pricaspian basin (Kazakhstan, e.g. Barde et al., 2002); the Sverdrup basin (Canada, Jackson and Harrison, 2006; 2013); the Canadian Maritime basin (Canada, Balkwill et al., 1989); German and North Sea Zechstein basins (Mohr et al., 2006; Jackson et al., 2010); Flinders ranges (Autralia, Rowan and Vendeville, 2006); Paradox basin (USA, Hudec and May, 1998); the Red Sea (Heaton et al., 1995); the Mid-Polish Trough (Poland, Krzywiecz, 2004); the Sivas Basin (Turkey, Ringenbach et al., 2013; Callot et al., 2014; Ribes et al., 2015; 2016).

Minibasins constitute a distinct type of sedimentary basin. As their name implies, they are much smaller than sedimentary basins (typically only a few kilometres in diameter at maximum) but despite their size, they do subside several orders of magnitude faster than most crustal basins (up to 10 km/m.y. (6 Mi/m.y) over short periods; Worrall and Snelson, 1989; Prather, 2000). High subsidence rates greater than 1 km/m.y.(0.6 Mi/m.y) can be sustained for several million of years producing Pliocene to Pleistocene minibasins thicker than 6km (3.8 Mi) in the deep part of the Gulf of Mexico (Hudec et al., 2008). Salt expelled from beneath a minibasin wells up around the minibasin margin, forming a network of salt walls or massifs

that partly or completely surround the minibasins. They display particular cartographic shapes, either sub-rounded or polygonal in the absence of external structural control (Rowan and Vendeville, 2006), or else more linear when regional tectonics interferes or developed along a slope (Nalpas and Brun, 1993). The rim of salt structures, welds and walls, which surround minibasins distinguishes them from other types of salt-withdrawal structures, which feed less-continuous networks of diapirs and walls. The network of salt related topographical highs relief in turns exert a strong influence on sediment distribution both in continental and deep marine setting, forcing fluvial channels as well as turbidity currents to deviate and pond in bathymetric low corresponding to already subsiding older basins. As the pounded minibasins are filled to their rim, they allow for sediments to spill toward downslope minibasins (Winker and Booth, 2000).

Minibasin paradox and early driving forces

A key issue raised during the last decade is the question of the driving force of minibasin inception and subsidence, which for long was described as purely gravitational and due to the weight of the sediments, supposed heavier than salt rock. Pure downbuilding nevertheless requires overcoming salt plasticity and sediments layers resistance in traction, and thus is generally triggered by external forces decreasing sediment resistance, such as erosion, compression, folding, tilting or extension, and gliding (e.g. Brun and Fort 2012).

Such a pattern of density inversion is classic in case of dense continental succession and “precompacted” sediments such as carbonates, and is necessary to form highly subsiding basins with steep walls bounded with halokinetic sequences. For marine clastic sediments lighter than salt mass, buoyancy alone can explain subsidence but cannot explain generation of accommodation space on top of the basin: the depocenter should migrate with time as the Archimede principle imposes that a positive bathymetric relief should pertain ontop of the depocenter. Sediment compaction curve, in the case of the Gulf of Mexico, indicate that a minimum thickness of 2300 meters (1.4 Mi) is needed to balance the salt typical density by the average density of the sedimentary column (Hudec et al., 2009). Such calculation, based solely on the Gulf of Mexico subsurface data, could in other settings underestimates the potential rapid diagenetic evolution of sediments, in particular through dense saline fluid percolation (see Amini, 2011), which have been observed in many wells drilled in the vicinity of salt masses, and would increase substantially the average sediment density at shallower depth.

Thus the idea of a minimum thickness needed to sustain minibasin subsidence is in fact not contradictory to data showing initiation of subsidence as early as sedimentation initiation (Worall and Snelson, 1989; Callot et al., 2012). Uneven sedimentation, creating mounds and topography by simple downbuilding and salt withdrawal, is a sufficient factor to explain the rapid and generalized subsidence of minibasins (Ings, 2006; Ings et al., 2010; Gradman and Beaumont, 2010; Rowan et al., 2012). Rajesh et al. (2012), based on numerical modelling results, estimated that the minimum time of uneven sedimentation required to initiate minibasin activity, due to sediment weight, and also the lateral variation of sediment thicknesses that generate pressure head and subsequent salt flow, to be less than 2My.

Minibasin kinematic from initiation to full development

The early deposits preceding or accompanying minibasin initiation may be initially, or after a small amount of time, unevenly distributed, defining the primary pattern of minibasins (as proposed for the early anhydrite deposition in the North Sea area above the Zechstein salt, see Stewart and Clark, 1999). Buoyancy controlled subsidence during early stage leaves a positive topographic relief in the core of the minibasin. Concomitantly, the salt flow from beneath the subsiding minibasin, even for minibasin lighter on average than salt initially, will initiate laterally to the minibasin salt highs and lows which in turn will compartmentalize new deposits (see Peel, 2014), due to the limited but existing initial subsidence. Both mechanisms will isolate the incipient minibasin and force the depocenter to migrate and expand the basin laterally. This initiation phase generates enlarged minibasins taht contain numerous internal unconformities, associated to wedge like basin edges thinning outward, as soon as the thickest parts of the basin reaches the density inversion depth on average. Then the subsidence will rapidly increase and focus on the basin center. The edges of the minibasin will subside less than the depocenter, favouring the localisation of sediments in the basin, and delineating uplifted ridges. Raised rims and stacked depotcentres are diagnostic of density driven subsidence, sometimes associated to a decrease in basin width when salt flow rate at surface becomes higher than sediment input (Hudec et al., 2009). At that time, the lateral salt wall will expand onto the adjacent basin, forcing the thinned rims to be backfolded rapidly if the salt feeder at depth is active, i.e. before the basin bottom is welded. Such a mechanisms is thus of prime interest to explain the developments of overturned basins edges, so called *megaflaps* (Dooley et al., 2009; Graham et al., 2012; Ringenbach et al, 2013; Alsop et al., 2015), following early basins subsidence.

Several alternative mechanisms will modulate the downbuilding mechanical evolution as minibasin are intrinsically non equilibrated, and will generate several secondary driving mechanisms, even in the absence of regional stresses such as shortening and extension, sediment progradation, and topographical gradients:

- Progradation of a topographic head related to sedimentary systems (Vendeville 2005), creates a slope and an uneven loading, for example at the mouth of distributary sediments systems (Jackson and Talbot, 1986; Ge et al., 1997; Hudec et al., 2007). In such a case, the depocentre location will migrate downdip the slope along with the prograding system, contrarily to the previous modes. Such mechanisms are particularly invoked in the German Zechstein basin (Ge et al., 1997; Vendeville, 2005).
- Secondly, salt wall and diapirs are considered weaker than minibasins (Schulz-Ela, 2003) and thus will shrink during shortening (Rowan and Vendeville, 2006; Callot et al., 2007 & 2012), producing local increase in salt topography and welding between basins. Even in case of minibasin lighter on average than surrounding rock salt, differential uplift related to shrinkage of the walls will leave minibasins as topographic lows allowing for sediments to accumulate during shortening. Minibasins subjected to shortening of their wall will themselves record deformation, as the rapidly deposited sediments are most probably poorly compacted and dewatered, thus allowing for local pore-fluid pressure to build up and potentially trigger important internal deformation (see a review in Hudec et al., 2007).
- A last type of mechanism is the decay of salt topography. This can be done either by extensional fall of diapirs, walls or any feeder structure, or else by migration of salt masse along slopes (Hudec 2011). Relaxation and extensional separation of salt diapir walls results in a local topographic low in between the original depocentres, which may localize a secondary minibasin in between primary ones, with a relict salt welds at the contact Salt flow along topography and salt flow within canopy are also responsible for local positive accommodation independently of sediment buoyancy, and will generate fixed depocentres above escaping salt sheet (see Hudec and Jackson 2006). In a mode similar to the sediment progradation and the salt escape, sub-salt deformation will also force salt migration and topographic decay at surface allowing for sedimentary systems capture.

Modelling methodology

This set of experiments was performed with the aim of reproducing minibasin geometry during simple downbuilding as well as their interactions, particularly during the formation of secondary minibasins and megaflaps. The modelling does not consider the triggering mechanism responsible for the minibasin initiation, and thus uses only dense analogue material for sediments, unrealistic for the inception stage of minibasin development, but more realistic for the mature stages. Minibasin development is thus related simply to passive sinking into the viscous layer. During the course of evolution of one model (3462), shortening has been applied to reproduce the contraction of the basin deeper parts and enhanced their interactions.

Analogue materials and scaling

Classic granular material obeying a Mohr-Coulomb failure criterion re used to simulate brittle sedimentary rocks. They consist of dry sand and corundum with grain size of 100 μm (0.004in, see Dooley et al., 2009; Callot et al., 2012). Their density contrast is large enough to be shown on the X-ray images. To simulate evaporite, the ductile analogue consists of silicone putty (PDMS, variety SGM 36 of Dow Corning) with Newtonian behaviour at low strain, a viscosity of $5x10^4$ $Pa.s^{-1}$ (7.2 $psi.s^{-1}$) and a density of 0.97. To these classic materials we have added pumice powder sieved to 150 μm (0.006in), which density is of the order of 0.6. It has a friction angle of μ=0.3, close to the glass microbead behaviour. Such material offers the advantage of being well imaged with X-ray tomography and thus easily underlines minibasin internal sedimentary structures. Its low density also lower the overall density of the brittle pile which is in general higher than expected from the scaling with respect to the silicone to salt density ratio, and thus magnifies the minibasin foundering, diapir and wall rises and salt expulsion (Dooley et al., 2007). The mixture of sand grain and silicone putty used is a 50% by volume mix, which give the mixture a density of 1.4, and a Newtonian viscosity of $1.5x10^5$ $Pa.s^{-1}$ (21.8 $psi.s^{-1}$) (see Callot et al., 2012 for the complete rheological analysis). It allows for a quite complete coupling between brittle and ductile levels, and thus magnifies the folding and distributed deformation processes as expected in cohesive sedimentary packages under confined conditions. It is in particular of prime importance if

testing the development of megaflaps, which in case of pure granular material will tend to produce slope avalanche rather than coherent structures.

Model scaling was done following the seminal work of Ramberg (1981; see also for the purpose of the deep salt basin modelling Dooley et al., 2009). We chose to scale 1km to a centimetre in the model (0.625Mi for 0.39in). The length ratio L_{model}/L_{nature} equals then 10^{-5}. Thus the stress ratio, which is simply the product of the length, density and gravity ratio, is $0.5x10^{-5}$. The viscosity of the silicone putty is 10^4 $Pa.s^{-1}$ (1.5 $psi.s^{-1}$), which is scaled to the viscosity of salt rock over geologic time scale, of the order of 10^{17} to 10^{18} (Weijermars, 1993; Van Keken et al., 1993). This scaling gives a viscosity ratio of 10^{-14} to 10^{-15}. The strain rate ratio is then the ratio between the stress and viscosity ratios, here $5x10^8$ to $5x10^9$. In the absence of inertial forces, the time ratio equals the viscosity ratio over the stress ratio, and is of the order of $2x10^{-9}$ to $2x10^{-10}$. Velocity ratio is simply the product of the length and strain rate ratios. For the purpose of minibasin evolution, experiments were performed over 4 days to account for the whole scenario of sedimentation. The experimental time of roughly 100 hours account thus for 6 to 60 My, which is reasonable considering the duration of minibasin development, of the order of a few My to a few tens of My.

Experimental set up and data capture

Analogue models were built in a 80x40 cm (31.5x15.7 in) deformation box (figure 2). The box is lying flat to avoid gravitational gliding as the box dimensions are far too small to properly represent the overall basin evolution during gliding, and to reproduce the basal shear drag at the right scale. Nevertheless a lateral moving edge allows performing shortening along the box long edge, and thus reproduces the progressive interactions between minibasins formation and down-dip contraction in the distal basin edge. A thick silicone layer represents the basal salt, which is supposed to be homogeneous. Brittle sediments, initially isopachous or not, are poured ontop of the silicone layer to initiate the silicone motion under differential loading only. Uneven sedimentation is used to shape sub-rounded early minibasins with long axis of the order of 8 to 10 km (5 to 6.5 Mi). The box size allows thus building a network of 6 to 12 initial minibasins, which subsidence immediately started, defining accommodation areas above and around minibasins, and silicone ridges in between. The model then freely evolved, the only external forcing being (1) addition of synkinematic layers made either of sand, pumice powder, or corundum in order to keep a flat free surface of the minibasins and model, and (2) for experiment 3462, lateral shortening by 4 cm (1.6 in) at a velocity of 2 mm (0.01

in) per hour (10% shortening) to simulate minibasin gliding and collisions in the deep basin. For experiment 3462, during the canopy emplacement, lateral source of sediment was used by sourcing the growing layers from the left hand side of the modelling bow to the right hand side, mimicking a progradation.

The deformation box is emplaced during the course of the experiment in a medical scanner to obtain real time non-destructive X-ray images of the model. Computerized X-ray tomography applied to analogue sandbox models allows us analysing the kinematic evolution and the three dimensional geometry without interrupting or destroying the model (Colletta et al., 1991). Scanner data are acquired along lines parallel to the box short side, one section every 3 mm (0.011 in), the image itself corresponds to a 2 mm (0.01 in) stripe of model. The 3D blocks are computed by image interpolation along the model long edges. In addition, serial cross-section images are also repeatedly measured during the course of the model evolution, in order to get 2D kinematic scenario of basin development.

Modelling result

Prekinematic layer rheology and thickness distribution

The rheology and thickness of the prekinematic layers is one of the key factors controlling the initiation of a minibasin. Two parameters have been investigated: (1) the rheology of the prekinematic layer, (2) the thickness of this layer. Rheology variations will be simulated by the use of three different sedimentary piles of variable mechanical architecture (figure 3). Either pure sand and corundum sequences with simple brittle behaviour, or pure viscous mix of sand and silicone, or last, composite layered sequences alternating brittle layers and viscous layers composed of a mixture of sand and silicone (see Callot et al., 2012). Here we also consider the rheology of the early deposits triggering the minibasin development, which may thus not be isopachous as discussed above, but rather define a pattern of evenly distributed depocentres.

A Pure viscous prekinematic layer (figures 3 and 4) rapidly thins while the minibasins sags and it smears to form a coating of silicone on the basins boundaries. The high ductility of this layer compared to the brittle layers, coupled to the weak basal silicone, allows for a rapid downbuilding, forming steep basin walls and stacked halokinetic sequences along the diapir walls, separating salt bodies from isopachous basin cores (figure 4). The overall shape of the minibasins is that of a bowl. If the sedimentation rate is faster than the

subsidence rate (controlled by the silicone flow and ability to flow at surface), the bowl shape minibasin will enlarge, forming edge prograding onto the lateral silicone structures. On the contrary, for sedimentation rates slower than the subsidence rate, the bowl shaped minibasin will shrink toward surface (figure 4).

The first type of evolution built thin basin edges which can later on evolve toward megaflaps, particularly if, as in the second type, high subsidence rates lead to the progressive invasion of the basin by a silicone glacier, pushing the initial sediment layers at its front. Along the diapir walls, each major sequence of deposition is terminating by a hook-like halokinetic sequence if the sediment deposition rate is close to balance the accommodation. At the time sedimentation overcomes the rate of silicone raise, layers onlap laterally over the silicone feeder, and build wedge-like halokinetic sequence. Eventually, if the accommodation becomes greater than the sedimentation rate, the basin edges evolve toward megaflap geometries.

A Mixed brittle and ductile prekinematic layer, either isopachous, or defining initial depocenters (figures 3 and 5), suffers a long phase of thinning before rupturing. The high viscosity of the sand and silicone mix (at 60% weight in sand, viscosity of 400 KPa.s (58 $psi.s^{-1}$), see Callot et al., 2012) precludes any rapid emergence of silicone at surface similarly to the pure viscous layer. But it also limits the development of overturned sequences (figure 5): In the case of initially non-isopachous layers, at roughly 30% of thinning, the silicone diapirs start to expand and overturn the basin edges which pinched-out originally ontop of the diapirs (figure 5A). This configuration then rapidly leads to the overturned sequence:. the thinned basin edges, rapidly evolve toward the megaflap configuration, with a quasi-isoclinal folding of the lower beds onto the basin surface. In the case of initially isopachous layers, the downbuilding phase first results in the boudinage of the layer (figure 5B), forming short, narrow basin edges, which cannot build megaflaps. The thicknesses variations seem to have a little impact on the evolution of the basin. Contrarily with the purely viscous prekinematic layer, for which the sedimentation rate is the most important factor controlling minibasin shape, this configuration shows that the rheology and thickness distribution of the prekinematic layer exert an important control on the size and shape of the megaflaps.

A Pure brittle layer evolution is displayed in figure 6. A brittle rheology still allows both for the development of halokinetic sequences along basin edges, lateral pinch-outs. During phases of increased silicone emission, although the rheology of the MB sequences is purely brittle, we observe a large development of overturned sequences flapped onto the basin centres. Thinning of the prekinematic layer occurs through the development of local arrays of

small normal faults, developed by bending and rapid lateral motion of the deposited sequence away from the growing diapir during inflation, and sometimes through avalanche of the granular material when the slope angle reaches the friction angle value. Contrarily to the previous models, the verticalized flanks and the megaflaps are more kinked than isoclinally folded owing to the brittle behaviour of the layers, and most generally associated to surface emission of silicone glaciers.

Deformation of a basin edges and formation of megaflaps

The classic modes of deformation observed in salt tectonics setting and described in our models are accompanied by megaflap geometries (Graham et al., 2012; Ringenbach et al., 2013; Callot et al., 2014) that were recently imaged and drilled in the Gulf of Mexico (Ringenbach et al., 2013). These have been defined as basin edges, thining toward the diapiric walls bounding the minibasin, folded and overturned during evaporite extrusion at surface, and flapped onto the basin centre. In that case, the minibasin geometry and the rheology of the oldest sediments strongly control the shape and size of the overturned structure. In the models, sedimentary sequences, thinning and overlapping over large silicone stocks with gentle slopes, lead to sharp and strong folding initiated by rupture of the thinned and tilted prekinematic layer (Figure 7).

Here the ratio between sedimentation and silicone flow appears to be an important but qualitative parameter, controlling the shape and the geometrical relationship of the megaflap to the minibasin stratal architecture (figures 7 and 8). Ductile and mixed ductile and brittle pre-kinematic layers allow both for (1) overturned flaps covered by extruded silicone in case of low sedimentation rate relative to the silicone extrusion rate, or else (2), vertical flaps at right angle to younger layers for sedimentation rate close to the accommodation rate. In the case of very high sedimentation rate, models show that overturned wings are an uncommon feature, as the basin edges rapidly prograde ontop of the silicone diapirs and thicken enough to limit the silicone diapir growth, forcing thick and narrow basin edge to develop. If the prekinematic layers are simply brittle, low sedimentation rate may lead to overturned flaps as soon as the silicone extrusion starts in between two basins. In the case of a balance between accommodation and sedimentation rates, the basin boundary do not develop overturned flaps but rather classic sequences of halokinetic growth strata, stacked along the vertical flap, which forms a coating of stretched and vertical sedimentary layers (see figure 7B for the case of pure brittle layer for instance).

Figure 8 shows three examples of imaged and drilled (data courtesy Cobalt Energy) basin boundaries from the deep GOM, illustrating various ratios of salt rise rate and sedimentation rates, resulting in contrasted basin edge shapes. The three lines shows the transition from a balanced input of sedimentation salt rise toward lower sediment input, allowing for the emplacement of megaflaps formed by folding and stretching of early sedimentary sequences.

Minibasins evolutions and interactions

Extrusion of silicone at surface leads to the building of a canopy that partially covers the primary minibasins. The canopy extend is variable but its emplacement is quite rapid, duration of the extrusion being of the order of a few tens of minutes (corresponding to 0.5 to less than 3My), and coalescence is generally reached after less than 2 hours (corresponding to 1 to 3 My) of surface flow (depending also on the lateral distance between feeders), a set of results comparable to published analysis of canopy dynamic (e.g. Hudec and Jackson, 2006; Dooley et al., 2012). During downbuilding and subsequent encapsulation below the canopy, minibasins collide, a phenomenon that will be amplified by any modification of the basin geometry and boundary conditions, such as gravitational gliding (and associated extensional and contractional domains) or shortening. Interactions is again increased when a second generation of minibasin forms above the canopy and start downbuilding and colliding on the formerly sunk minibasin.

Several situations may arise: basin contact during subsidence will create a differential motion between parts of the minibasin, and lead to rotation, folding associated to migration of depotcentre, and potentially basin damage through fracturation and faulting.

Rotations

Rotations are observed mostly as a response asymmetric collision, generating a pivot point forcing the subsiding basin to subside only from one side (figure 9A). Rotation can be enhanced due to progradational sedimentation, amplifying the initial rotation of the minibasin through lateral migration of the depot centre, generating a torque and, if minibasins are not already colliding, favouring rotation. Such mechanism is not favoured as the brittle material used (sand and corundum) are heavier than expected with respect to silicone, thus leading to downbuilding of the minibasin rather than rotation, due to the enhanced subsidence which compensate rotation by focusing sediment flux. But considering the poorly compacted early sediments, in the deep Gulf of Mexico for instance, one would expect rapid lateral migration

of depocenters as the deposited layers, although subsiding in the evaporite, will leave a bathymetric relief. Rotations are then amplified by lateral contacts between minibasins, forming pivot points around which a minibasin will rotate during subsidence (figure 9B). Shortening and potential contact between lateral edges of minibasins also favour minibasins rotations. High amount of rotation are observed, up to 90°.

Folding

Minibasins, particularly their lateral edges, are prone to folding during settling against another minibasin, a pattern again amplified by regional shortening, either due to gravitational gliding or to regional shortening (figure 10). In the presented line, the secondary and third sets of minibasins are progressively sinking into the successive canopies, developing major depocenter above the available main feeder (figures 10B and C), and welded contact onto the primary minibasins (figure 10A). This differential subsidence forces the development of folds between depocenters, similarly to the seismic line in figure 10D, which shows the complex refolding of the Plio-Pleistocene minibasins above the Miocene canopy, as well as the welded contacts between the various generation of minibasins. Folding can easily lead to duplication of the basin sedimentary sequence (figure 11) developing horizontal welding zones at the base and at the top of primary minibasins progressively encapsulated into the original silicone layer. Laterally, folded zone may pass to basin disruption into two sub-basins, separated by a silicone ridge, or by a fault zone. The cross-sections in figure 11-1 shows how a flat secondary minibasin can laterally evolve toward a strongly folded bridge joining two depocenters (figures 11-2, 3, 4), partially broken by crestal extensional collapse (figure 11-4). The bridge itself disappears laterally (figure 11-5), evolving in a thrust like contact emplacing the right end side minibasin onto the left end side main depocenter, thus duplicating the sequence with an internal weld. Folding can occur at surface and not only at depth during subsidence and interaction between basins. This is demonstrated by the development of syntectonic wedges of slumped material evidencing avalanche processes related to topography creation with non-cohesive material. Such lateral evolution of a fold commonly lead to the development of welded zone, thrusted or collapsing, and is a feature commonly imaged in salt provinces (e.g. Rowan et al., 2000; Rowan et al., 2012; Callot et al., 2014).

Faulting

Eventually a last type of mechanical interaction is faulting (Figure 12). Extensional forces along the outer-arc extensional domain of folded minibasin is a common feature, similar to the turtle back anticlines. In that case, the fault pattern is directly related to the

folding geometry, which can be controlled either by pure gravitational subsidence or by basin interactions. Considering a complex array of minibasins, basin collision during subsidence can also create fault arrays in the subsiding minibasin to accommodate its lateral contacts with other minibasins and related stress increase (figures 12A and B). Point-centred fault-arrays (i.e. related to a single contact point, figure 12A) and folding-related fault-array (Figure 12-(3)) are two common geometries observed. An extreme case is the basin rupture, a case leading to the separation of small basinal blocks (figure 12A and C), which can be transported away from the parent basin over large distances, sometimes above the basin core, a pattern that has been proposed in some cases from seismic images in the Gulf of Mexico (figure 12D)

Overall pattern of minibasin distribution (figure 13)

At the scale of the whole deformation box, the model evolution is based on an initial set of 8 early minibasins separated by silicone walls. A first episode of canopy building allows for a second phase of minibasin generation, with freely developed early minibasins (i.e. with completely random generation through homogeneous sand sprinkling), forming a polygonal complex array of wall-and basin structures (sensu Harrison and Jackson 2013). During that phase, primary silicone feeders can localize accommodation and building of secondary minibasins, as the feeders can be rapidly disconnected from the parent feeding-layer. This is particularly obvious in the depth slice of figure 13A, where the NS-elongated, festooned basins (marked by stars), located at the cross section junction in the North East corner of the image, show three main depocenters separated by thinner basin sequences, the three depocenters corresponding to the main silicone ridges separating originally the primary minibasins, i.e. the initial feeders, marked by an F in the cross-section of figures 13C and D and in the time slice of figure 13A.

This model also illustrates the complexity of minibasin's distribution of orientations, as in any section observed one could find merely any type of basins shape, contacts and orientations as well, with both verticalized primary minibasins, flat lying secondary minibasins resting gently onto the former completely subsided primary minibasins, and secondary basins having suffered variable rotations during settling. In the cross-section of figure 13C, the model geometry is quite similar to the proposed interpreted seismic line from the Gulf of Mexico (figure 13E) displaying four primary minibasins (denoted by a star on figure 13E) overlain by five secondary minibasins (marked by two stars in figure 13E), the central one including a lateral, early salt sheet disrupting the sedimentary succession. The

early minibasins have variable stratigraphic extend, as the central one is interpreted as a late one emplaced in an early, rapidly inhibited feeder. The model also illustrates the contrasted timescale for minibasin evolution. Primary as well as secondary minibasins rapidly evolve during initial downbuilding, creating welds and complex architecture of contacts. But following this initial phase, the minibasins still evolve much slowly, but continuously through compaction, indentation and fracturation, as seen for the late section on figure 13B2.

Analogies with salt structures and salt provinces

Analogies with known minibasin provinces

There are few minibasins provinces at outcrop, and most of the existing data comes from the subsurface. The models presented here show quite interesting analogies with previously described minibasin provinces: the Flinders ranges (Southern Australia), the Sverdrup basin (Arctic Canada) and the Sivas basin (Turkey). These three examples display a very comparable pattern of minibasin geometry, size and shapes, and cartographic distribution, similar by many aspects to the proposed modeling.

The Proterozoic Flinders Ranges (Southern Australia) are composed of a beautifully outcropping amalgamation of salt walls and former diapirs shaping polygonal minibasins, showing evidence of allochtonous salt sheets or even canopies (e.g. Rowan and Vendeville, 2006; Hearon et al., 2014). Nevertheless, outcrop conditions, and present day level of exposure within the canopy itself preclude delineating former or buried minibasins. A second field analogue of minibasin province developed onto a canopy, recently described in the Axel Heiberg Island (Jackson and Harrison, 2006; 2013), is exceptionally well exposed due to arctic dry climate. In that particular case, a buried canopy is proposed, based on field evidence (1) of the shallow depth of detachement for the development of equant egg-shaped minibasins separated by polygonal salt walls, (2) consistent emplacement stratigraphic level of exposed allochthonous evaporite (Harrison and Jackson 2013).

The Sivas basin (central Anatolian Plateau, Turkey) is the last regional outcropping minibasin province (Ringenbach et al. 2013; Callot et al., 2014; figure 14). In the Sivas Basin, minibasins, gypsum diapirs, glaciers, evaporite walls and and welds, and potential local small canopies are located in a foreland type setting between the Pontides belt to the north and the Tauride belt to the South (Temiz et al., 1996; Callot et al., 2014). The 35x25 km (13.5x9.7

Mi) core of the basin shows polygonal to sub-circular minibasins bounded by gypsum walls, and partially covered by remobilized gypsum (either sedimentary or flowage). The minibasins are filled by Mid-Oligocene to Early Miocene clastics (fluvial silts and sandstones), marls, and lacustrine to marine limestones, the thickness of which may reach 4 kilometres (Ribes et al., 2015). The stratal architecture along evaporite walls records the progressive subsidence of the minibasins, with strong rotation of beds, unconformities and local reworking of evaporites. Within the basins, the sediments show lateral thickness variations and spectacular angular unconformities (Ribes et al., 2015; 2016; Kergaravat et al., submitted). In particular, as discussed for the present study modelled minibasins, the early stage of basin evolution is associated to complex migration of the depocenters, delineating laterally wedges of sediments thinning onto the gypsum walls, illustrating the difficulty for the low-compaction, early deposited, layers to subside completely. On the contrary, the upper parts of the early, continental, minibasins sedimentary sequences, if at outcrop, show vertically stacked halokinetic sequences (hook-like, see Ribes et al., 2015; 2016). Also the regional tectonic setting has a quite important impact on the Sivas area, with the continuous shortening associated to (1) the Taurus retro arc mountain building, and (2) to the development of the Pontides belt later on, the minibasins appear to be quite comparable to the geometries developed in our modelling. This suggests that the boundary forces have a small impact compared to the downbuilding and silicone flow on local, basin scale or halokinetic sequence scale geometries.

Flaps and unusual geometries

At smaller scale, the most amazing salt tectonic structure reproduced here are the overturned flaps, which are now more and more imaged seismically in offshore areas (e.g. Ringenbach et al., 2013). It is also known from outcrops, in the Southern French Alps (Graham et al., 2012), from the Flinders Ranges (Southern Australia, Hearon et al., 2015), and from the Dead See diapirs (Alsop et al., 2015). They were a primary objective of the modeling as well. The large imprint of salt tectonics on the European margin of the Southern Alps has been recognized for a quite long time (Mascle et al., 1988; Dardeau et al., 1990). The later documented in great details the numerous outcropping diapirs, which were strained during the various stages of the Pyrenean and Alpine orogenic phase. All these works were based on classic arguments in favor of salt tectonics, namely locally reduced stratigraphic succession, reworked Triassic salt material, local unconformities and truncations, sharp facies

changes and slumps, debris flows. Recently, Graham et al. (2012) revisited the area and proposed that triassic salt not only fed salt diapirs but also allochtonous salt nappes associates to reduced sedimentary succession, some of them forming overturned flaps during diapir evolution. The described objects are comparable to what has been imaged in the deep Gulf of Mexico seismic (figure 10) and modeled repeatedly in our experiments (figure 9). This field example, in marine setting, is to our knowledge the only one described together with the Sivas basin flap of the Karayün minibasin in continental setting (Ringenbach et al., 2013; Callot et al., 2014), the Proterozoic salt flaps in the Willouran Ranges (Southern Australia, Hearon et al., 2015), and the Dead Sea basin (Alsop et al., 2015). This kind of structures recall at a smaller scale the flap structures described on the fold limbs in the Iranian Zagros (Sherkati and Letouzey, 2004). In the experimental cases, aerial inflation of the slightly buried diapir is responsible for the building of the flap, and can be obtained solely from the downbuilding scenario of basin subsidence. But increased salt motion is clearly a factor strongly favouring the flap development through basin collision, local or regional shortening related to tectonic phases or gravitational gliding at the toe of a passive margin. The present day natural flaps have been observed in various settings: passive margin reactive diapirism (Southern Alps, France; Graham et al., 2012) and toe-thrust advances linked to sedimentary progradational systems (Hearon et al., 2015), compressive retro arc setting (Sivas Basin, Turkey; Callot et al., 2014 ; Kergaravat et al., submitted), Extensional faulting (Dead sea, Alsop et al., 2015). It appears that shortening is not a preferred or common mechanism of megaflap development, but may greatly enhanced their development. The timing of development has also an impact as porrly compacted young sediments are prone to more efficient deformation, enhanced by the mobile fluid content (Graham et al. 2012; Alsop et al., 2015).

Conclusions

X-ray tomography of scaled sand-silicone models allows to built 3D time evolution of minibasins and minibasin province, and particularly the evolution of the basin limits and their interactions. Models are simply based on successive steps of sand layers sedimentation over an initially thick isopachous layer of silicone. The three major steps of minibasin evolution are observed, namely (1) the depocenter initiation and successive avulsions; (2) the downbuilding phase; and (3) the collapse and progressive death of the basin after basal contact is achieved, and or burial beneath a sediment coffin or silicone glacier. Folding, faulting and overturning of thin basin edges are classic features that compare well to field and

drilled subsurface objects. Minibasin interactions result in basin deformation, which are not linked to regional processes but rather to local geometries.

Acknowledgements

J.-P. Callot acknowledges the financial support of Cobalt Energy while performing analogue experiments at IFP Energies Nouvelles, and a Total Grant for the Structural Geology chair at Université de Pau et des Pays de l'Adour, and permission to publish the results. We thank Jean-Marie Mengus (IFP-EN) for invaluable technical and experimental knowledge in analogue modeling. M. Hudec, an anonymous reviewer and associate editor R. Groshong are thanked for the comments that improved the early version of the manuscript. Dr M.S.N. Carpenter, a professional translator, is acknowledged for post-editing the manuscript. F. Whitehurst is thanked for her involvement in improving the final manuscript.

Figure captions

Figure 1 : Typical cross-section (modified from a seismic line showing a minibasin surrounded by salt walls and diapirs on both sides, and by salt welds along the bottom edge of the basin (modified from Hudec et al., 2011).

Figure 2 : Experimental set-up: Medical scanner used (A) to image the experimental box (B) Plane surface view of the experimental box during the course of the experiment. Note the silicone glaciers (arrow) partially covered by thin sand layers. (C) Typical cross sections acquired during the course of the experiment and showing the kinematic evolution of the model at a given location.

Figure 3: Three examples of rheological layering in cross section used during the experiments: A Anisopachous prekinematic layers with mixed rheology; b Anisopachous prekinematic layer with purely viscous rheology; C Isopachous prekinematic layers with mixed rheology (see text for explanations). Right end side: Stratigraphic column for each experiment. Thicknesses vary laterally. Sykinematic thicknesses are highly variable and are not delineated.

Figure 4 : (A) Three final minibasin geometries from experiment 3351 (see also figure 5). Minibasin geometries vary depending on the ratio between sedimentation rate and local silicone rate of raise. Note the successive Halokinetic sequences (HS) along side the basin walls. Scale bar is 1 cm. (B) : Examples from the Angolan margin of a closing minibasin (left), and a steady state minibasin (middle) and from the Gulf of Mexico of a closing minibasin showing a central sequence at steady state.

Figure 5 : Time evolution of cross sectional view of two minibasin settings (experiments 3351 and 3354 respectively). A: Interstratified prekinematic layers of viscous and brittle materials, initially with variable thicknesses. B: Interstratified prekinematic layers of viscous and brittle materials, initially of constant thickness. Initial wegde-like succession evidences a higher rate of sedimentation compared to the silicone extrusion rate. A strong decrease of sedimentation rate compared to silicone

extrusion rate is necessary to form tightly folded overturned flaps. Scale bar is 2cm. Note that thick, constant thickness, pre-kinematic layers do not favour establishment of mega-flap geometries.

Figure 6 : Pure brittle model showing the development of secondary minibasins allowing for the folding of the basin edges during a decrease of sedimentation rate. Dotted lines denote the location of the cross sectional views and of the time slices. Scale bar is 1 cm. Purely brittle layers favor rigid tilting of megaflaps, indicated by arrows.

Figure 7 : (A) Typical geometries of minibasins depending on the prekinematic layer stratification and the ratio between sedimentation rate and local accommodation rate controlled by silicone rise. (B) Kinematic evolution of a flap. Stratigraphic columns depict the rheological layering of the models. Initial thicknesses vary laterally. Synkinematic thicknesses are highly variable.

Figure 8 : Three example from of mega-flaps the Gulf of Mexico. The shape of the flap directly depends on the ratio between sedimentation and salt extrusion rates.

Figure 9: Examples of rotated minibasins. (A) Rotation due to the progradation of sediments, leading to an asymmetric minibasin (1) progressively sunk along its right side. (B) Rotation around a contact pivot point, minibasin (2) is originally symmetric but now close to vertical. Pink color denotes first stage minibasins; Yellow color second stage minibasins, deposited in the first canopy; Natural colors stand for the third stage minibasins, deposited in the second, late canopy.

Figure 10 : Three examples of folded minibasins. A: Folded thinner zone separating two main depocentres within the middle minibasin, and localizing subsequent younger minibasins; B: Differential sinking of depocentres connected by thinner basin edges which are folded during settling (the dark area is an air bubble produced by sand layers during their vertical and tectonic compaction); C: Third stage minibasin showing synkinmatic slumped sand in the fold core, evidencing aerial development of the fold. Color code as in figure 10. Lower image is an interpreted line from the deep GOM showing similar complex pattern of minibasin folding.

Figure 11: Along strike evolution of a folded minibasin (model 3432). The cross-sections illustrate the passage from a disrupted basin (cross section 1) to a sigmoid fold (cross sections 2 to 4) with a welded core, ending a in thrust-like weld emplacing the right end side part of the minibasin over its left counter part through a weld (cross section 5). Color code as in figure 10. Slumped material in the fold core (cross section 3) is evidence for aerial development of the fold.

Figure 12 : Three examples of faulting in secondary minibasins during foundering (color code as in figure 10). (A) Complete rupture of basin edges and transport of a basin raft, thrusted onto its mother basin (1). (B) and (C) Fault development during folding, either related to contact between basins and associated stress increase (2) or to folding (3). (D) kinematic scenario from the deep GOM showing the transport, folding, and near rupture of the small basin extension during diapir building.

Figure 13 : (A) Time slice of the model 3433 at the end of the 4 days experiment, with location of the cross section shown on the right (B), scale bar 3cm (color code as in figure 10). Depth-slice A shows the location of the minibasins developed within the feeder of the second canopy (stars). Cross-sections B and C show the interactions between primary minibasins (pink), early settled on the basement, and secondary minibasins (yellow), faulted and folded. Inline section D (imaged along strike of the deformation box) illustrates the thickening of the late stage minibasin within feeders

zones (F). (C) Example of an interpreted seismic line from the Gulf of Mexico (courtesy Western Geco, see also Callot et al., 2014), showing a quite comparable pattern of minibasin spatial distribution, with 4 primary minibasins (marked by an asterisk) separated by the Miocene canopy from five secondary minibasins (marked by two asterisks), one having sunk within the main feeder and being now covered by an other minibasin. Scale bar 4km, F stands for feeder.

Figure 14: The case of the central Sivas Basin, a minibasin province. (A) Regional composite lithostratigraphic column showing the average thickness of the various stratigraphic units in the central Sivas Basin. (B) Geological map of the central Sivas Basin, showing location of salt outcrops (black and grey) and the polygonal geometry of gypsum walls surrounding the mini-basins (labeled by their names). Black dotted lines denote angular unconformities related to internal structuration of mini-basins during downbuilding, and internal wedging of syn-halokinesis sediments are evidenced by the thin continuous lines delineating sedimentary bedding. D: Evaporite diapir; G: Evaporite glacier; Wa: evaporite wall; We: evaporite weld. Modified from Ribes et al., 2016.

References

1. Alsop, G.I., Weinberger, R., Levi, T., Marco, S., Deformation within an exposed salt wall: Recumbent folding and extrusion of evaporites in the Dead Sea Basin, Journal of Structural Geology (2014), doi: 10.1016/j.jsg.2014.11.006.
2. Amini, A., 2011. Red colouring of the Upper Red Formation in central part of its basin Central Iran. J. Sci. I.R. Iran, 12, 145-156.
3. Balkwill, H.R., and Legall, F.D., 1989, Whale Basin, offshore Newfoundland: Extension and salt diapirism, in Tankard, A.J., and Balkwill, H.R., eds., Extension Tectonics and stratigraphy of the North Atlantic margins: American Association of Petroleum Geologists Memoir 46, p. 233–245.
4. Barde, J.P., Gralla, P., Harwijanto, J., and Marsky, J., 2002, Exploration at the eastern edge of the Precaspian basin: Impact of data integration on Upper Permian and Triassic prospectivity: American Association of Petroleum Geologists Bulletin, v. 86, p. 399–415.
5. Burollet, P. F., 1975, Tectonique en radeaux en Angola: Bulletin de la Société Géologique de France, v. 17, p. 503– 504.
6. Callot, J.P., Jahani, S., Letouzey, J., 2007. The role of pre-existing diapirs in fold and thrust belt development. In: Lacombe, O., Roure, F., Lavé, J., Vergés, J. (Eds.), Thrust Belts and Foreland Basins from Fold Kinematics to Hydrocarbon Systems: Frontiers in Earth Sciences. Springer, Berlin, Heidelberg, pp. 309–325.
7. Callot, J.P., Trocmé V., Letouzey J., Albouyi, E., S. Jahani, S. Sherkati, 2012. Pre-existing salt structures and the folding of the Zagros Mountain. From: Alsop, G. I., Archer, S. G., Hartley, A. J., Grant, N. T. & Hodgkinson, R. (eds) 2012. Salt Tectonics, Sediments and Prospectivity, Geological Society, London, Special Publications, 363, 545–561. http://dx.doi.org/10.1144/SP363.27.
8. Callot, JP., Ribes, C., Kergaravat, C., Bonnel, C., Temiz, H., Poisson, A., Vrielynck, B., Ringenbach, JC., 2014, Salt tectonics in the Sivas Basin (Turkey), Walking across salt wall and minibasins. Bull. Soc. Geol. France, 185, 1,.
9. Cobbold, P.R., Szatmari, P., Demercian, L.S., Coelho, D., and Rossello, E.A., 1995, Seismic and experimental evidence for thin-skinned horizontal shortening by convergent radial gliding on evaporites, deep-water Santos Basin, Brazil, in Jackson, M.P.A., Roberts, D.G., and Snelson, S., Salt tectonics: A global perspective: American Association of Petroleum Geologists Memoir 65, p. 305–321.
10. Colletta, B., Letouzey, J., Pinedo, R., Ballard, JF., Balé, P. (1991). Computerized X-ray tomography analysis of sandbox models: Examples of thin-skinned thrust systems. Geology, 19, 1063-1067.

11. Coward, M., and Stewart, S. (1995). Salt influence structures in the Mesozoic-Tertiary cover of the Southern North Sea, U.K. In Jackson, M.P.A., Roberts, D.G., and Snelson, S. (eds.), Salt Tectonics : a global Perspective. Am. Assoc. Petrol. Geol. Mem. 65, 229-250.
12. Diegel, F. A., J. F. Karlo, D. C. Schuster, R. C. Shoup, and P. R. Tauvers, 1995, Cenozoic structural evolution and tectonostratigraphic framework of the northern Gulf Coast continental margin, in M. P. A. Jackson, D. G. Roberts, and S. Snelson, eds., Salt tectonics: A global perspective: AAPG Memoir 65, p. 109–151.
13. Dooley, T.P., Jackson, M.P.A., Hudec, M.R., 2006. Allochthonous salt extrusion, roof dispersion, and intrusive import and export of salt in squeezed stocks (abs.). American Association of Petroleum Geologists Annual Convention 15, 27.
14. Dooley, T.P., Jackson, M.P.A., Hudec, M., 2009. Inflation and deflation of deeply buried salt stocks during lateral shortening. J. Struct. Geol., 31, 582-600.
15. Dooley, T.P., Hudec, M.R., and Jackson, M.P.A. The structure and evolution of sutures in allochthonous salt. Am. Assoc. Petrol. Geol., 96, 1045-1070.
16. Davison, I., Bosence, D ., Alsop, G.I., Al-Aawah, M.H., 1996. Deformation and sedimentation around active Miocene salt diapirs on the Tihama plain, northwest Yemen. In Alsop, I., Blundell, D.J. and Davison, I. (Eds.), Salt Tectonics, Geological Society of London, Spec. Pub. 100, 23-40.
17. Jackson, M.P.A., Talbot, C.J., 1986. External shapes, strain rates, and dynamics of salt structures. Geological Society of American Bulletin 97, 305-323.
18. Jackson, M. P. A., Vendeville, B. C. and Schultz-Ela, D. D. (1994) Structural dynamics of salt systems. Annual Review of Earth and Planetary Sciences 22, 93-177.
19. Jackson, M.P.A. and Harrison, J.C., 2006. An allochthonous salt canopy on Axel Heiberg Island, Sverdrup Basin, Arctic Canada. Geology, 34, 1045-1048.
20. Fort, X., Brun, J.P., Chauvel, F., 2004. Salt tectonics on the Angolan margin, synsedimentary deformation processes. Am. Assoc. Petrol. Geol. Bull., 88, 1523-1544.
21. Fort, X., and Brun, JP., 2012. Kinematics of regional salt flow in the northern Gulf of Mexico. Geol. Soc. Spec. Pub., 363, 265-287, doi: 10.1144/ SP363.12.
22. Ge, H., Jackson, M.P.A., and Vendeville, B.C., Kinematics and dynamics of salt tectonics driven by progradation. AAPG , v. 81, p. 398-423, 1997.
23. Giles, K.A., Lawton, T.F., 1999. Attributes and evolution of an exhumed salt weld, La Popa basin, northeastern Mexico. Geology 27, 323‐326.
24. Giles, K.A., and Lawton, T.F., 2002. Halokinetic sequence stratigraphy adjacent to the El Papalote diapir Northeastern Mexico. Am. Assoc. Petrol. Geol. Bull., 86, 823-840.
25. Graham, R., Jackson, M. Pilcher, R., and Kilsdonk, W. 2012 Allochthonous salt in the sub-Alpine fold-thrust belt of Haute Provence, France, Geological Society, London, Special Publications, doi:10.1144/SP363.30.
26. Hearon, T.E., Rowan, M.G., Lawton, T.F., Hannah, P.T., and Giles, K.A., 2014. Geology and tectonics of Neoproterozoic salt diapirs and salt sheets in the eastern Willouran Ranges, South Australi. Basin Res., 27, 183-207.
27. Ings, S.J., 2006. Passive Continental Margin Salt Tectonics: Numerical Modelling, Analytical Stability Analysis, and Applications to the Scotian Margin, Offshore Eastern Canada. Ph.D. Thesis. Dalhousie University, Halifax, Nova Scotia, pp. 352.
28. Ings, S.J., Beaumont, C., 2010. Shortening viscous pressure ridges, a solution to the enigma of initiating salt 'withdrawal' minibasins. Geology 38, 339–342.
29. Harrison, J.V. and Falcon, N.L., 1936. Gravity collapse structures and mountain ranges, as examplified in south-western Iran. Quarter. J. Geol. Soc. London, 92, 91-101.
30. Harrison, J.C., and Jackson, M.P.A., 2013. Exposed evaporite diapirs and minibasins above a canopy in the central Sverdrup Basin, Axel Heiberg Island, Arctic Canada. Basin Res., in press.
31. Heaton, R.C., Jackson, M.P.A., Bamahmoud, M., and Nani, A.S.O., 1995, Superposed Neogene extension, contraction, and salt canopy emplacement in the Yemeni Red Sea, in Jackson, M.P.A., Roberts, D.G., and Snelson, S., eds., Salt tectonics: A global perspective: American Association of Petroleum Geologists Memoir 65, p. 333–351.

32. Hudec, M.R., and May, S.R., 1998, The Courthouse syncline: A Gulf of Mexico–style minibasin exposed in the Paradox Basin, Utah [abs.]: American Association of Petroleum Geologists Annual Convention Offi cial Program, v. 7, CD-ROM.
33. Hudec, M.R., and Jackson, M.P.A., 2004, Regional restoration across the Kwanza Basin, Angola: Salt tectonics triggered by repeated uplift of a metastable passive margin: American Association of P etroleum Geologists Bulletin, v. 88, p. 971–990, doi:10.1306/02050403061.2012, 363:595-615.
34. Hudec, M.R., Jackson, M.P.A., 2006. Advance of allochthonous salt sheets in passive margins and orogens. AAPG Bulletin 90 (10), 1535–1564.
35. Hudec M.R., and Jackson, M.P.A., 2007. Terra Infirma : Understanding salt tectonics. Earth Science Review, 82, 1-28.
36. Hudec M.R., and Jackson, M.P.A., 2009. Interaction between spreading salt canopies and their peripheral thrust system. J. Struct. Geol., 31, 1114-1129.
37. Hudec, M.R., Jackson, M.P.A., Schultz-Ela, D.D., 2009. The paradox of minibasin subsidence into salt: clues to the evolution of crustal basins. Geological Society of America Bulletin 121, 201–221.
38. Jackson, M.P.A., Harrison, J.C., 2006. An allochthonous salt canopy on Axel Heiberg Island, Sverdrup Basin, Arctic Canada. Geology 34, 1045–1048.
39. Jackson, C. A.-L., Kane, K.E., Larsen, E., 2010. Structural evolutuon of minibasins on the Utsira High, northern North Sea ; Implications for Jurassic sediment dispersal and reservoir distribution. Petrol. Geosci., 16, 105-120, doi : 10.1144/1354-079309-011.
40. Krzywiec, P., 2004. Basement vs. salt tectonics and salt‐sediment interaction—case study of the Mesozoic evolution of the intracontinental Mid-Polish Trough. In: Post, P.P., Olson, D.L., Lyons, K.T., Palmes, S.L., Harrison, P.F., Rosen, N.C. (Eds.), Salt‐Sediment Interactions and Hydrocarbon Prospectivity: Concepts, Applications, and Case Studies for the 21st Century. 24th Annual Gulf Coast Section SEPM Foundation Bob F. Perkins Research Conference, CD ROM.
41. Lehner, P., 1969, Salt tectonics and Pleistocene stratigraphy on continental slope of northern Gulf of Mexico: American Association of Petroleum Geologists Bulletin, v. 53, p. 2431–2479, doi: 10.1306/5D25C945-16C1-11D7-8645000102C1865D.
42. Mascle, G., Arnaud, H., et al., 1988. Tethyan rifting and alpine folding in the french alps. Bull. Soc. Geol. Fr., 8, 747-758.
43. Mohr, M., Kukla, P.A., Urai, J.L., and Bresser, G., 2005, Multiphase salt tectonic evolution in NW Germany: Seismic interpretation and retro-deformation: International Journal of Earth Sciences, v. 94, p. 917–940, doi: 10.1007/s00531-005-0039-5.
44. Nalpas, T., Brun J.-P., 1993. Salt flow and diapirism related to extension at crustal scale. Tectonophys. 228, 349-362.
45. Peel, F.J., 2014, How do salt withdrawal minibasins form? Insigths from forward modelling, and implications for hydrocarbon migration. Tectonophysics, 630, 222-235.
46. Poisson, A.M., Guezou, J.C., Öztürk, A., Inan, S., Temiz, H., Gursöy, H., Kavak, K., & Özden, S. 1996. - Tectonic setting and evolution of the Sivas Basin, Central Anatolia, Turkey.- Inter. Geol. Rev. 38, 838–853.
47. Ribes, C., Kergaravat, C., Bonnel, C., Crumeyrolle, P., Callot, JP., Poisson, A., Temiz, H., Ringenbach, J.C., 2015, Fluvial sedimentation in a salt-controlled mini-basin: stratal patterns and facies assemblages, Sivas Basin, Turkey. Sedimentology, doi:10.1111/sed.12195.
48. Ribes, C., Kergaravat, C., Kergaravat, C., Crumeyrolle, P., Lopez, M., Bonnel, C., Poisson, A., Kavak, K., Callot, J.-P., and Ringenbach, J.-C., Factors controlling stratal pattern and facies distribution of fluvio-lacustrine sedimentation in the Sivas minibasins, Oligocene (Turkey). Basin Research, 1-26, doi: 10.1111/bre.12171.
49. Rouby, D., Raillard, S., Guillaucheau, F., Bouroullec, R., Nalpas, T., 2002. Kinematics of a growth fault/raft system on the west African margin using 3D restoration. J. Struct. Geol., 24, 783-796.

50. Rowan, M.G., Lawton, T.F., Giles, K.A., Ratliff, R.A., 2003b. Near-salt deformation in La Popa basin, Mexico, and the northern Gulf of Mexico: a general model for passive diapirism. AAPG Bulletin 87, 733–756.
51. Rowan, M.G., Peel, F.J., Vendeville, B.C., 2004. Gravity-driven fold belts on passive margins. In: McClay, K.R. (Ed.), Thrust Tectonics and Hydrocarbon Systems. AAPG Memoir 82, 157–182.
52. Rowan, M.G., Vendeville, B.C., 2006. Foldbelts with early salt withdrawal and diapirism: physical model and examples from the northern Gulf of Mexico and the Flinders Ranges, Australia. Marine and Petroleum Geology 23 (9–10), 871–891.
53. Rowan, M.G., Peel, F.J., Vendeville, B.C., Gaulier, V., 2012. Salt tectonics at passive margins : Geology versus models – Discussion. Marine Petrol. Geol., doi:10.1016/j.marpetgeo.2012.04.007.
54. Prather, B.E., 2000, Calibration and visualization of depositional process models for above-grade slopes: A case study from the Gulf of Mexico: Marine and Petroleum Geology, v. 17, p. 619–638, doi: 10.1016/S0264- 8172(00)00015-5.
55. Sherkati, S., Letouzey, J. and Frizon de Lamotte, D., 2006. Central Zagros fold and thrust belt (Iran): New insights from seismic data, field observations, and sandbox modelling. Tectonics, 25, TC 4007, doi.org/10.1029/2004TC001766.
56. Spathopoulos, F., 1996, An insight on salt tectonics in the Angola Basin, South Atlantic, in D. J. Blundel, G. I. Alsop, and J. Davison, eds., Salt tectonics: Geological Society (London) Special Publication 100, p. 153– 174.
57. Stewart, S.A., and Clark, J.A., 1999, Impact of salt on the structure of the central North Sea hydrocarbon fairways, in Fleet, A.J., and Boldy, S.A.R., eds., Petroleum geology of northwest Europe: Proceedings of the 5th Conference: London, Geological Society of London, p. 179–200.
58. Talbot, C.J. (1998). Extrusions of Hormuz salt in Iran. In: Blundell, D.J., Scott, A.C. (Eds.), Lyell, the Past is the Key to the Present. Geological Society Special Publication, vol. 143, pp. 315–334.
59. Temiz, H. 1996. - Tectonostratigraphy and thrust tectonics of the Central and eastern parts of the SivasTertiray Basin (Turkey). - Inter. Geol. Rev., 38, 957-971.
60. Trusheim, F., 1960, Mechanism of salt migration in northern Germany: American Association of Petroleum Geologists Bulletin, v. 44, p. 1519–1540.
61. van Keken, P.E., Spiers, C.J., van Den Berg, A.P., Muyzert, E.J., 1993. The effective viscosity of rocksalt: implementation of steady state creep laws in numerical models of salt diapirism. Tectonophysics 225, 457–475.
62. Vendeville, B.C, 2005. Salt tectonics driven by sediment progradation. Part I: mechanics and kinematics. Am. Assoc. Petrol. Geol. Bull., 89, 1071-1079.
63. Volozh, Y.A., Talbot, C.J., and Ismail-Zadeh, A.T., salt structures and hydrocarbons in the Pricaspian basin. Am. Assoc. Petrol. Geol., 87, 313-332.
64. Weijermars, R., 1986. Flow behaviour and physical chemistry of bouncing putties and related polymers in view of tectonic laboratory applications. Tectonophysics 124, 325–358.
65. Weijermars, R., Jackson, M.P.A., Vendeville, B.C., 1993. Rheological and tectonic modeling of salt provinces. Tectonophysics 217, 143–174.
66. Winker, C.D., and Booth, J.R., 2000, Sedimentary dynamics of the salt-dominated continental slope, Gulf of Mexico: Integration of observations from the seafloor, near-surface, and deep subsurface, in Weimer, P., Slatt, R.M., Coleman, J., Rossen, N.C., Nelson, H., Bouma, A.H., Styzen, M.J., and Lawrence, D.T., eds., Deepwater reservoirs of the world, 20th Annual Research Conference Proceedings: Houston, Texas, Society of Economic Paleontologists and Mineralogists, Gulf Coast Section, p. 1059–1086.
67. Worrall, D.M., and Snelson, S., 1989, Evolution of the northern Gulf of Mexico, with emphasis on Cenozoic growth faulting and the role of salt, in Bally, A., and Palmer, A., eds., The geology of North America—An overview: Boulder, Colorado, Geological Society of America, v. A, p. 97–138.

Figure 1

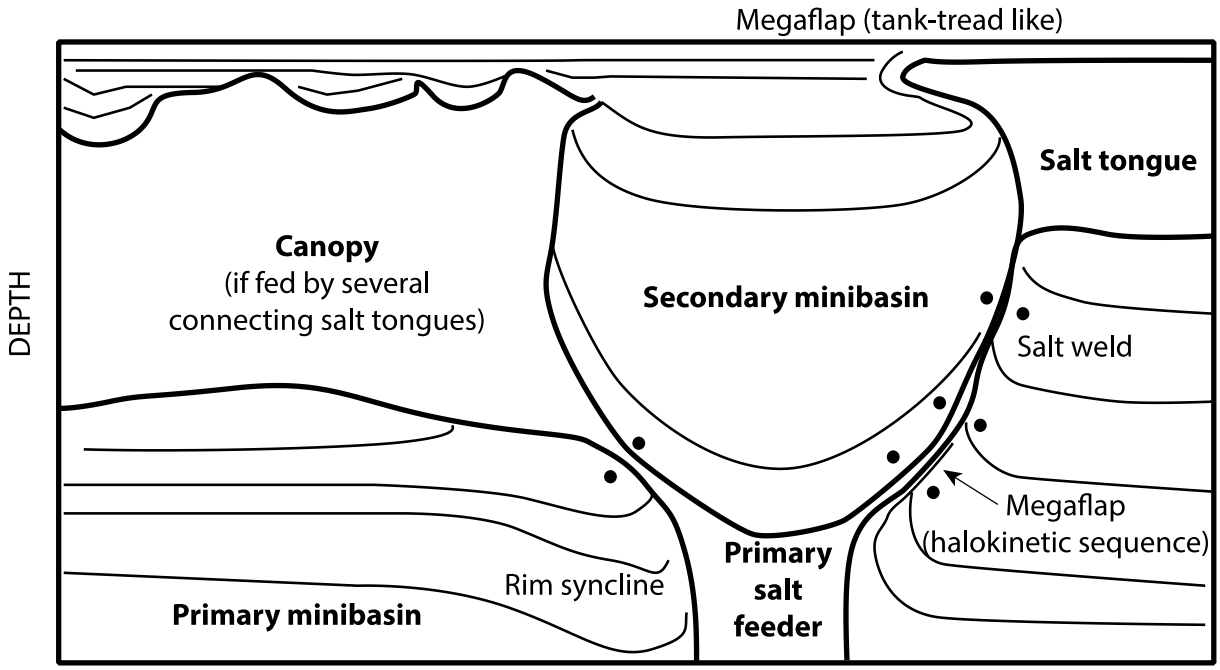
Megaflap (tank-tread like)
DEPTH
Salt tongue
Canopy
(if fed by several
connecting salt tongues)
Secondary minibasin
Salt weld
Megaflap
(halokinetic sequence)
Primary
salt
feeder
Rim syncline
Primary minibasin

Figure 2

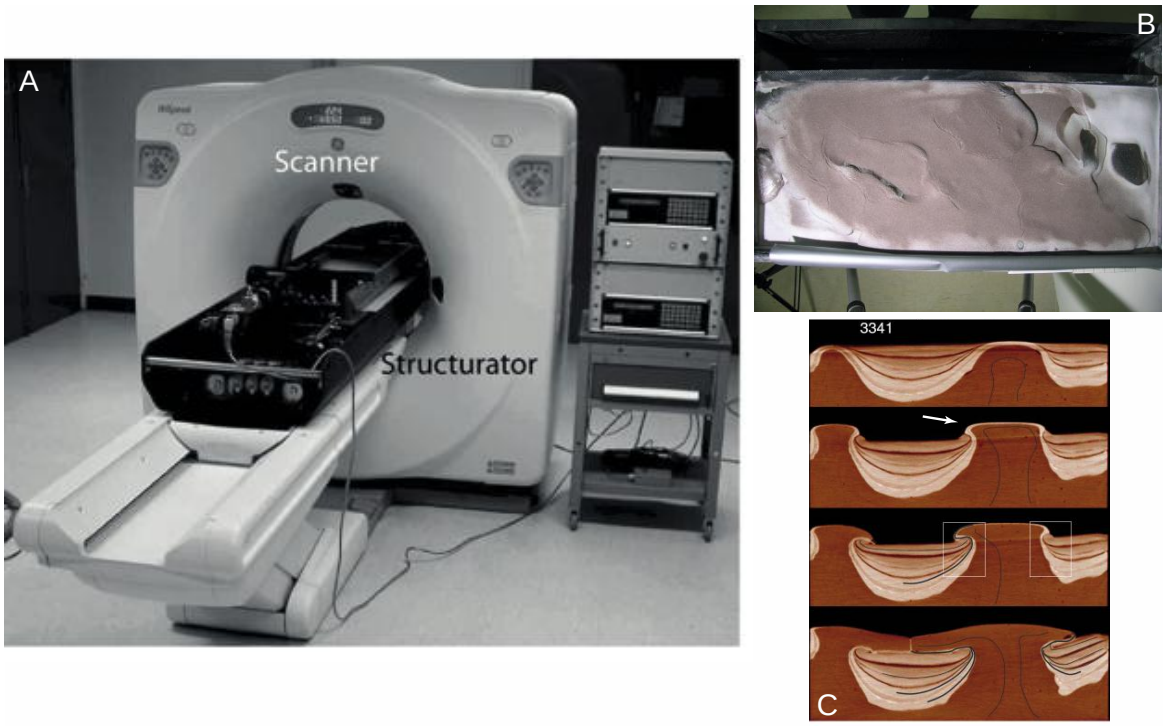

Figure 3

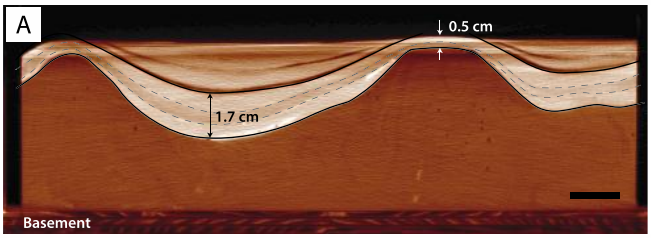

Exp. 3341 - Anisopachous prekinematic layers

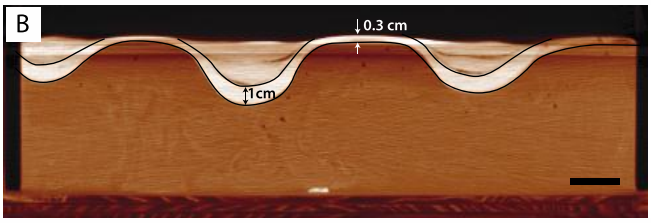

Exp. 3351 -Anisopachous prekinematic layers

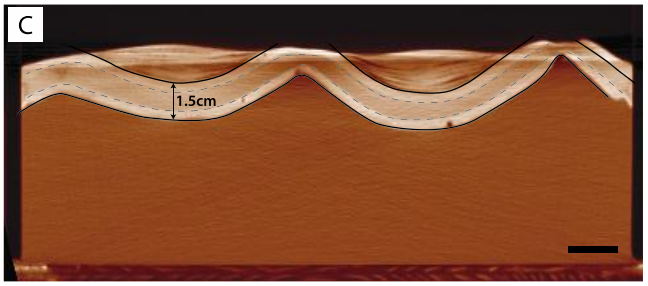

Exp. 3351 - Isopachous prekinematic layers

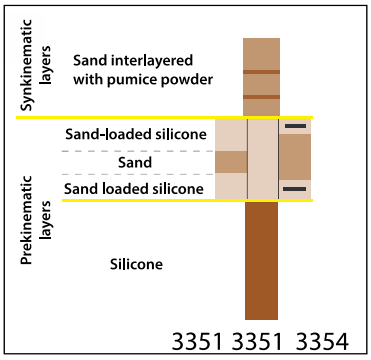

Figure 4

A - Experimental results

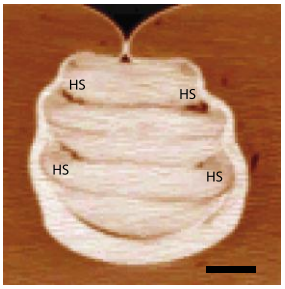

Low sedimentation rate

- Closure of the minibasin

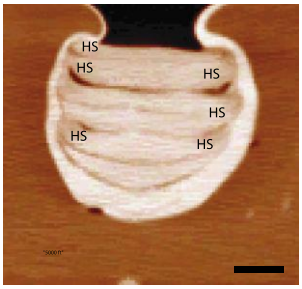

Medium sedimentation rate

- Steady-state growth of the minibasin

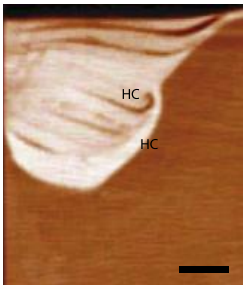

High sedimentation rate

- Enlargment of the minibasin

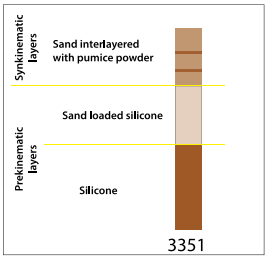

B - Seismic images of natural examples

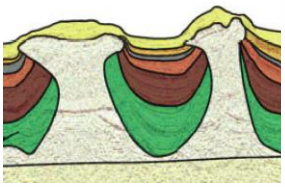

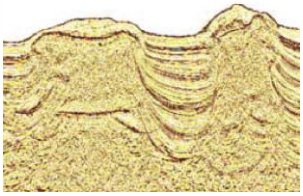

Angolan margin rafted domain
(modified from Fort and Brun, 2004)

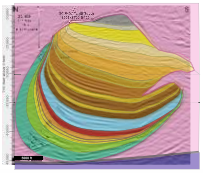

Gulf of Mexico
(Courtesy Colbalt Energy)

Figure 5

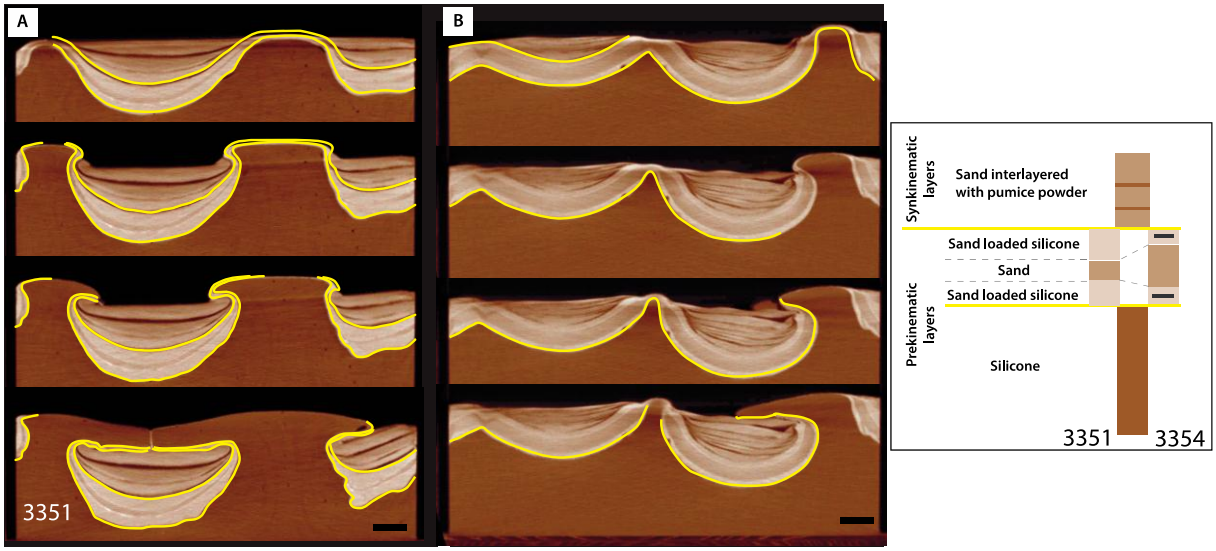

Initially NON ISOPACHOUS
Mixed brittle - ductile layers

Initially ISOPACHOUS
Mixed brittle - ductile layers

Figure 6

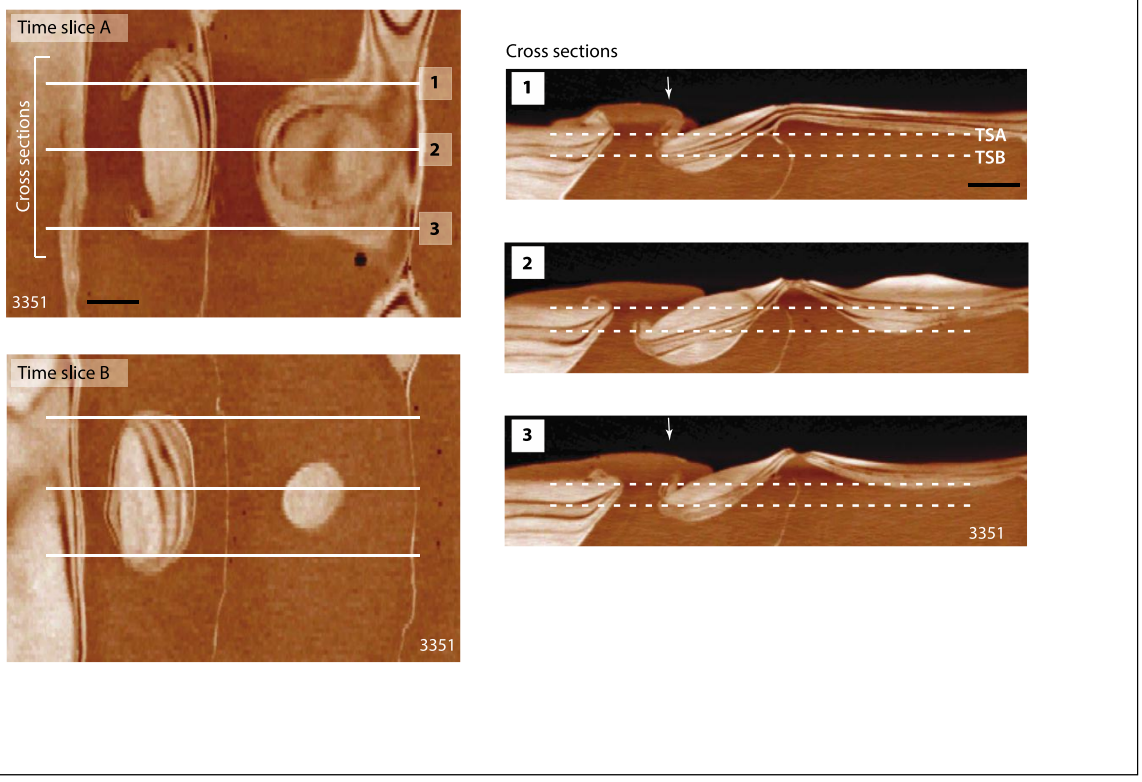
Time slice A
Cross sections
1
2
3
3351
Time slice B
3351
Cross sections
1
TSA
TSB
2
3
3351

Figure 7

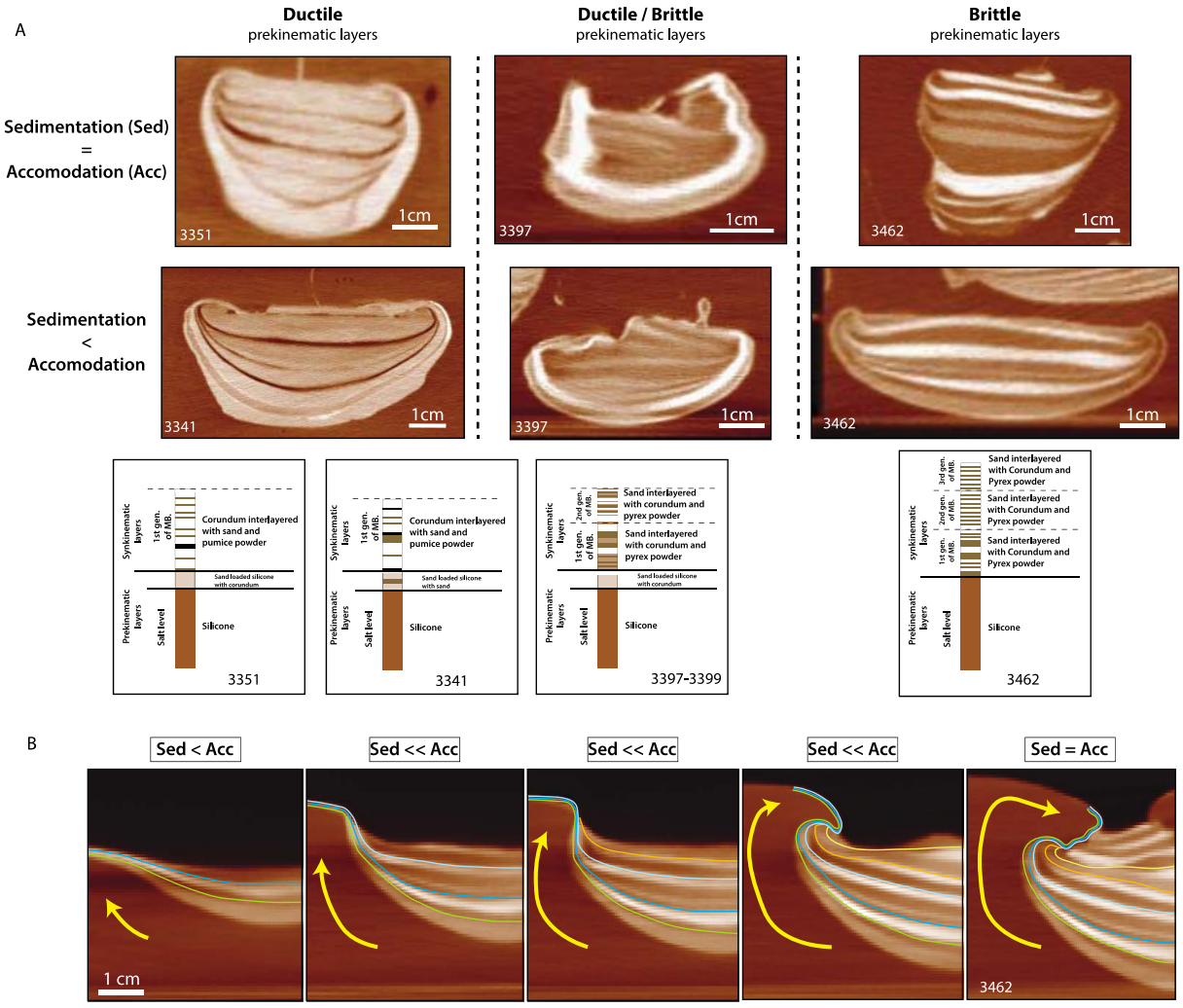
A
Ductile
prekinematic layers
Ductile / Brittle
prekinematic layers
Brittle
prekinematic layers
Sedimentation (Sed)
=
Accomodation (Acc)
Sedimentation
<
Accomodation
3351
3397
3462
3341
3397
3462
1cm
Synkinematic layers
Prekinematic layers
Salt level
Silicone
Corundum interlayered with sand and pumice powder
Sand loaded silicone with corundum
Sand loaded silicone with sand
Sand interlayered with corundum and pyrex powder
Sand interlayered with Corundum and Pyrex powder
1st gen. of MB.
2nd gen. of MB.
3rd gen. of MB.
3351
3341
3397-3399
3462
B
Sed < Acc
Sed << Acc
Sed << Acc
Sed << Acc
Sed = Acc
1 cm
3462

Figure 8

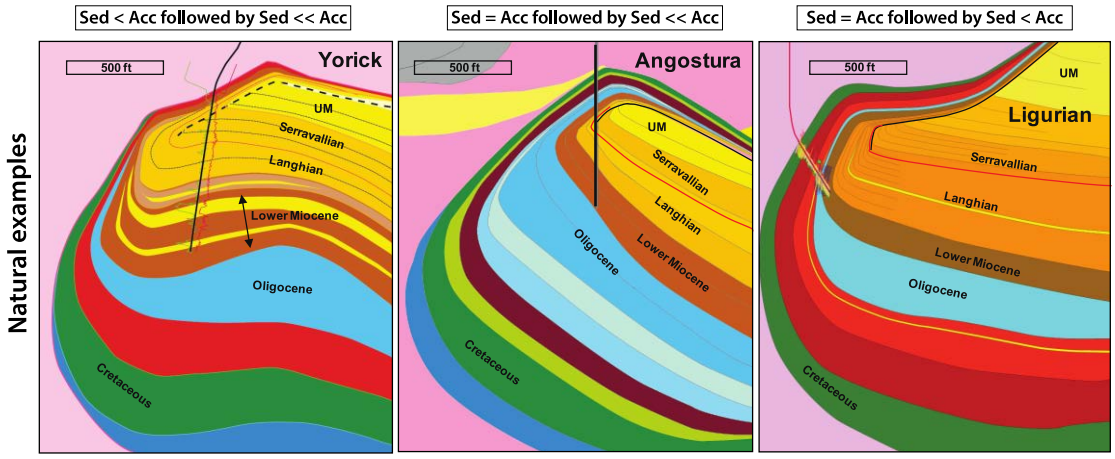
Sed < Acc followed by Sed << Acc
Sed = Acc followed by Sed << Acc
Sed = Acc followed by Sed < Acc
Natural examples
500 ft
Yorick
UM
Serravallian
Langhian
Lower Miocene
Oligocene
Cretaceous
500 ft
Angostura
UM
Serravallian
Langhian
Oligocene
Lower Miocene
Cretaceous
500 ft
UM
Ligurian
Serravallian
Langhian
Lower Miocene
Oligocene
Cretaceous

Figure 9

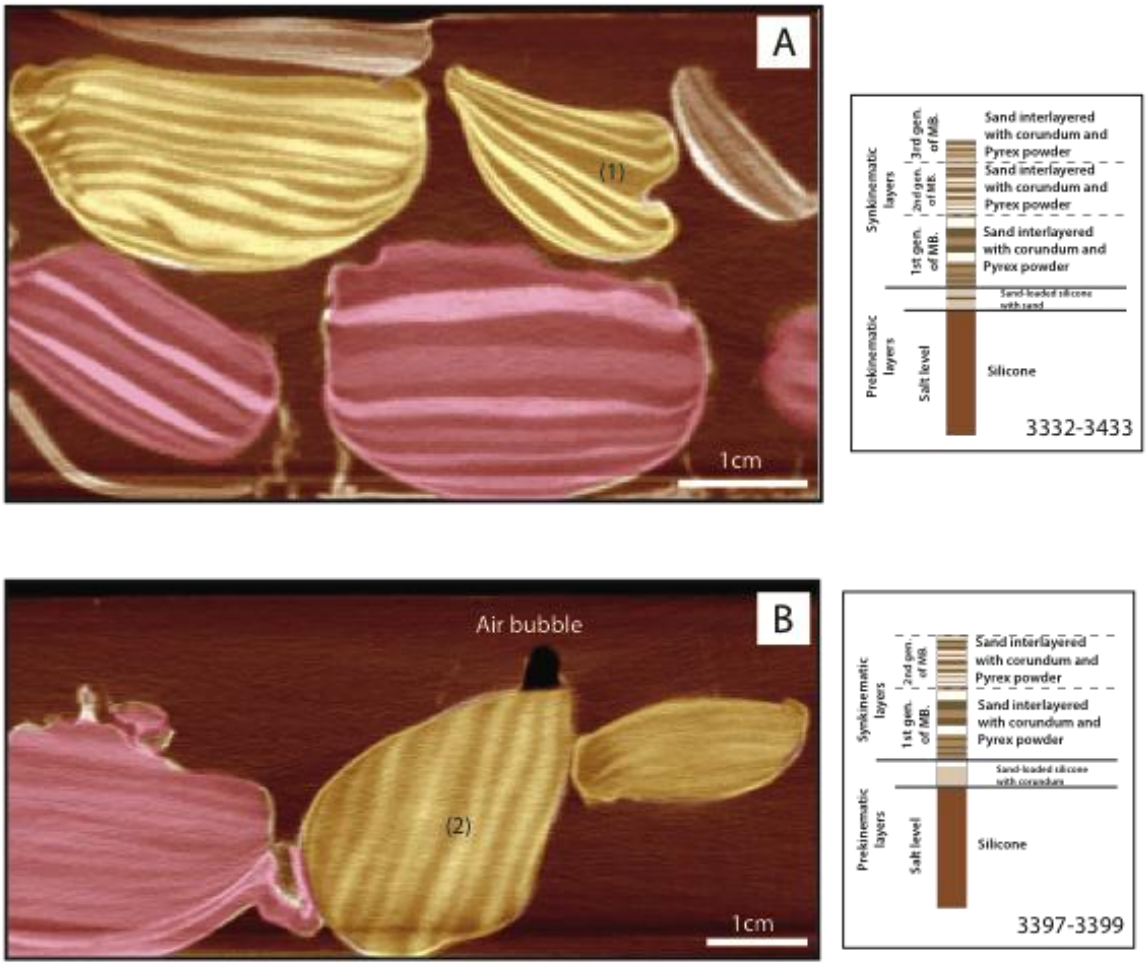
A
(1)
1cm
Synkinematic layers
3rd gen. of MB.
2nd gen. of MB.
1st gen. of MB.
Sand interlayered with corundum and Pyrex powder
Sand interlayered with corundum and Pyrex powder
Sand interlayered with corundum and Pyrex powder
Sand-loaded silicone with sand
Prekinematic layers
Salt level
Silicone
3332-3433
B
Air bubble
(2)
1cm
Synkinematic layers
2nd gen. of MB.
1st gen. of MB.
Sand interlayered with corundum and Pyrex powder
Sand interlayered with corundum and Pyrex powder
Sand-loaded silicone with corundum
Prekinematic layers
Salt level
Silicone
3397-3399

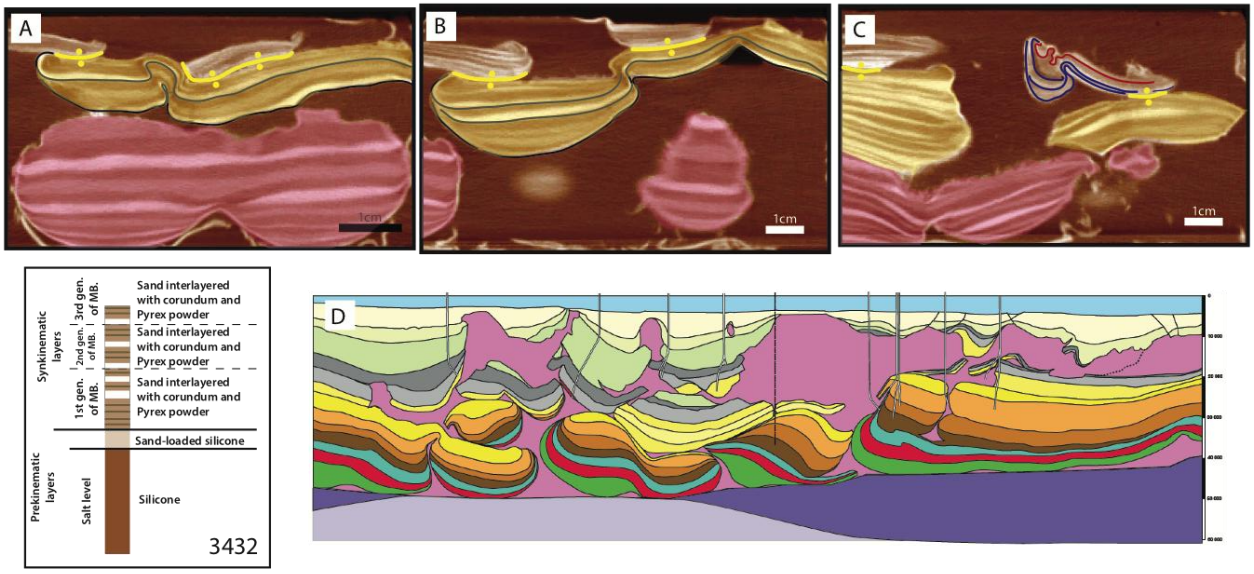
A
1cm
B
1cm
C
1cm
Synkinematic layers
3rd gen. of MB.
2nd gen. of MB.
1st gen. of MB.
Sand interlayered with corundum and Pyrex powder
Sand interlayered with corundum and Pyrex powder
Sand interlayered with corundum and Pyrex powder
Sand-loaded silicone
Prekinematic layers
Salt level
Silicone
3432
D

Figure 10

Figure 11

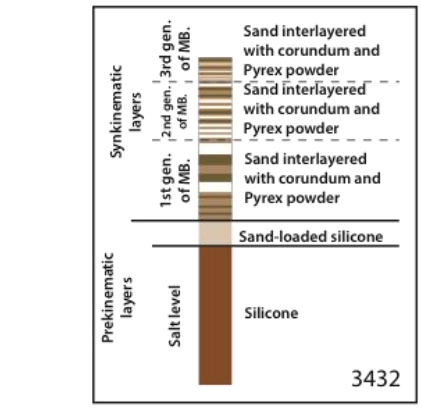

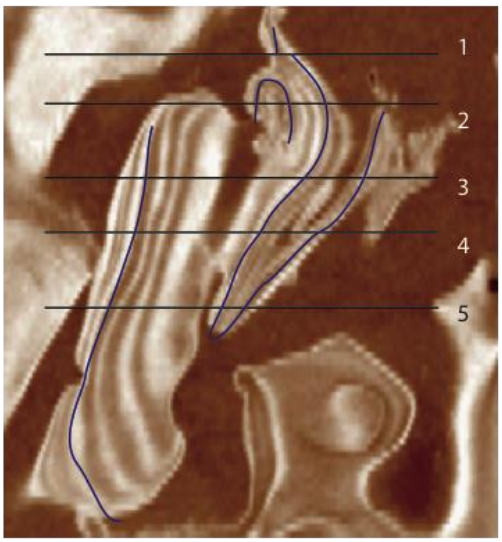

Depth slice

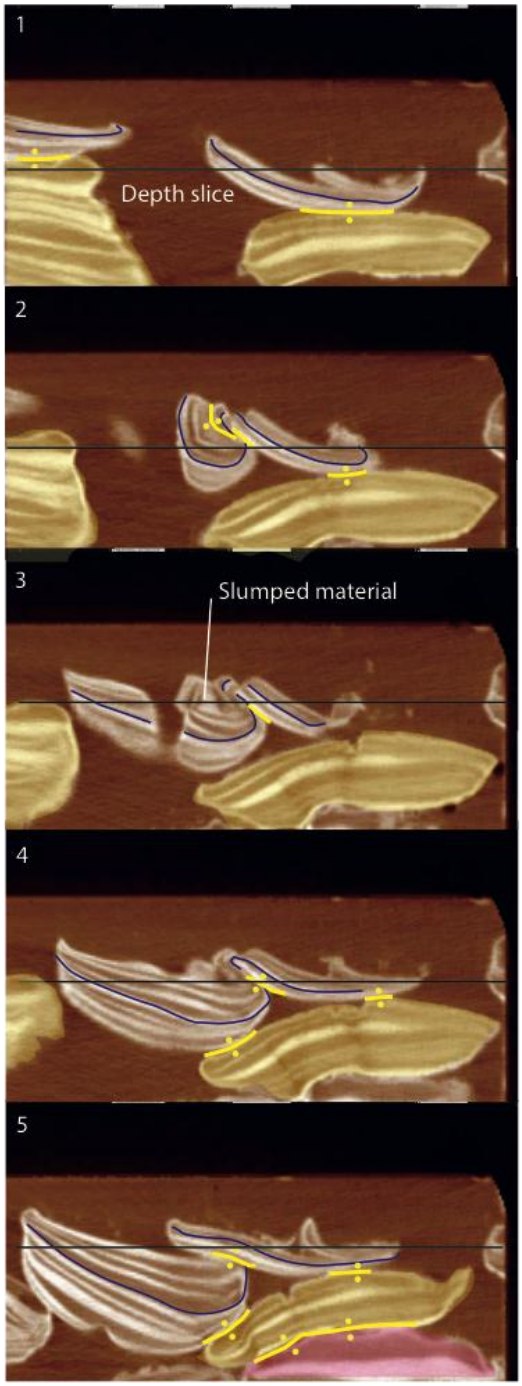

Figure 12

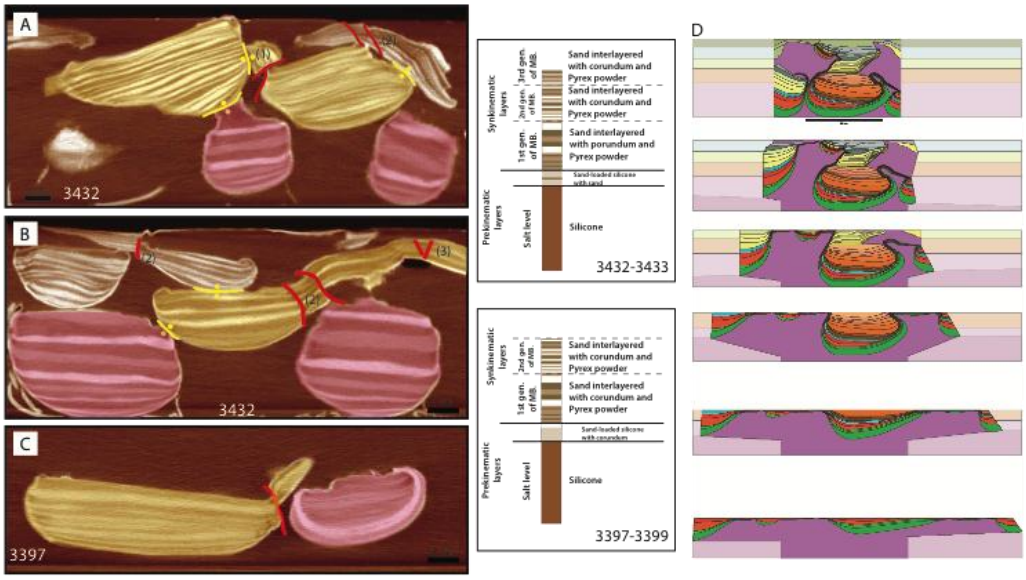
A
3432
B
3432
C
3397
Synkinematic layers
1st gen. of MB.
2nd gen. of MB.
3rd gen. of MB.
Sand interlayered with corundum and Pyrex powder
Sand interlayered with corundum and Pyrex powder
Sand interlayered with porundum and Pyrex powder
Sand-loaded silicone with sand
Prekinematic layers
Salt level
Silicone
3432-3433
Synkinematic layers
1st gen. of MB.
2nd gen. of MB.
Sand interlayered with corundum and Pyrex powder
Sand interlayered with corundum and Pyrex powder
Sand-loaded silicone with corundum
Prekinematic layers
Salt level
Silicone
3397-3399
D

Figure 13

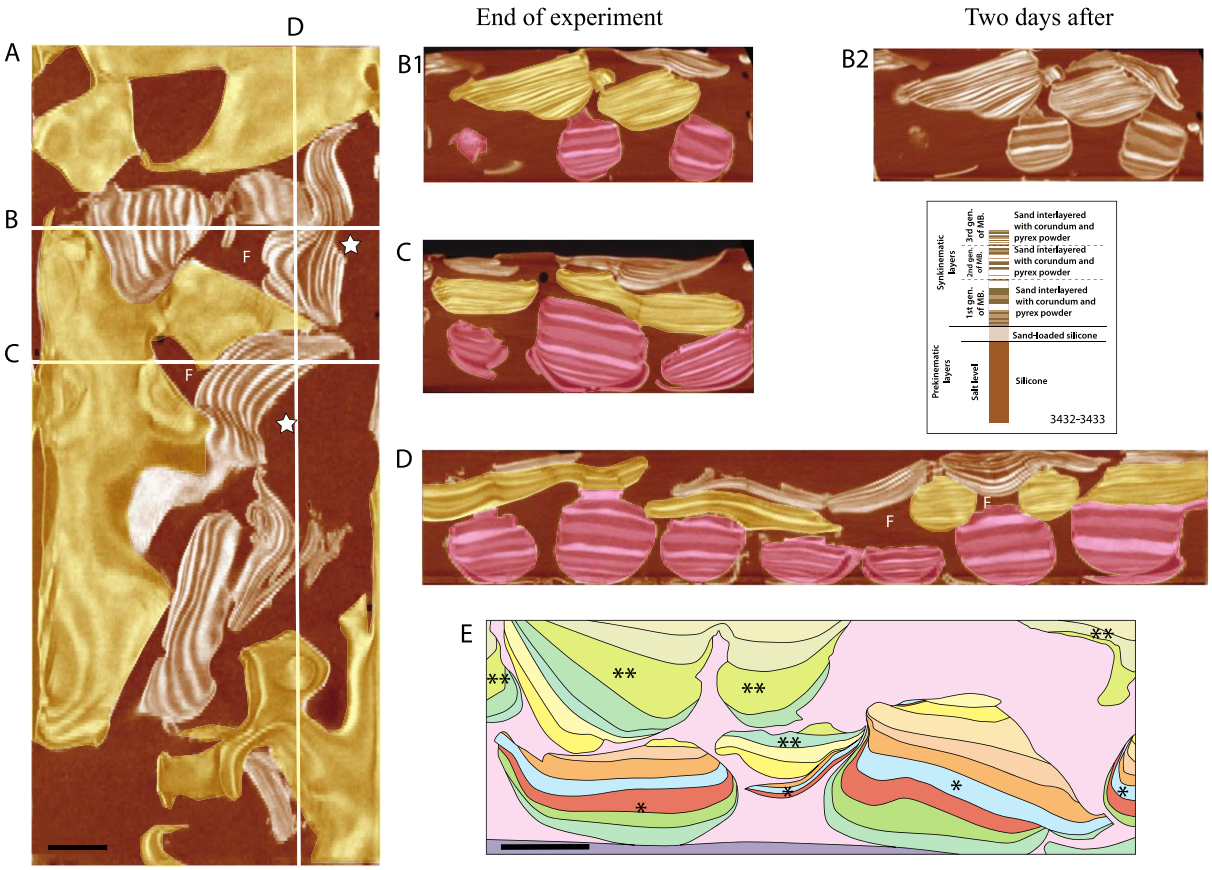
D
End of experiment
Two days after
A
B
C
B1
B2
C
D
E
F
F
F
Synkinematic layers
3rd gen. of MB.
2nd gen. of MB.
1st gen. of MB.
Sand interlayered with corundum and pyrex powder
Sand interlayered with corundum and pyrex powder
Sand interlayered with corundum and pyrex powder
Sand-loaded silicone
Prekinematic layers
Salt-level
Silicone
3432-3433

Figure 14

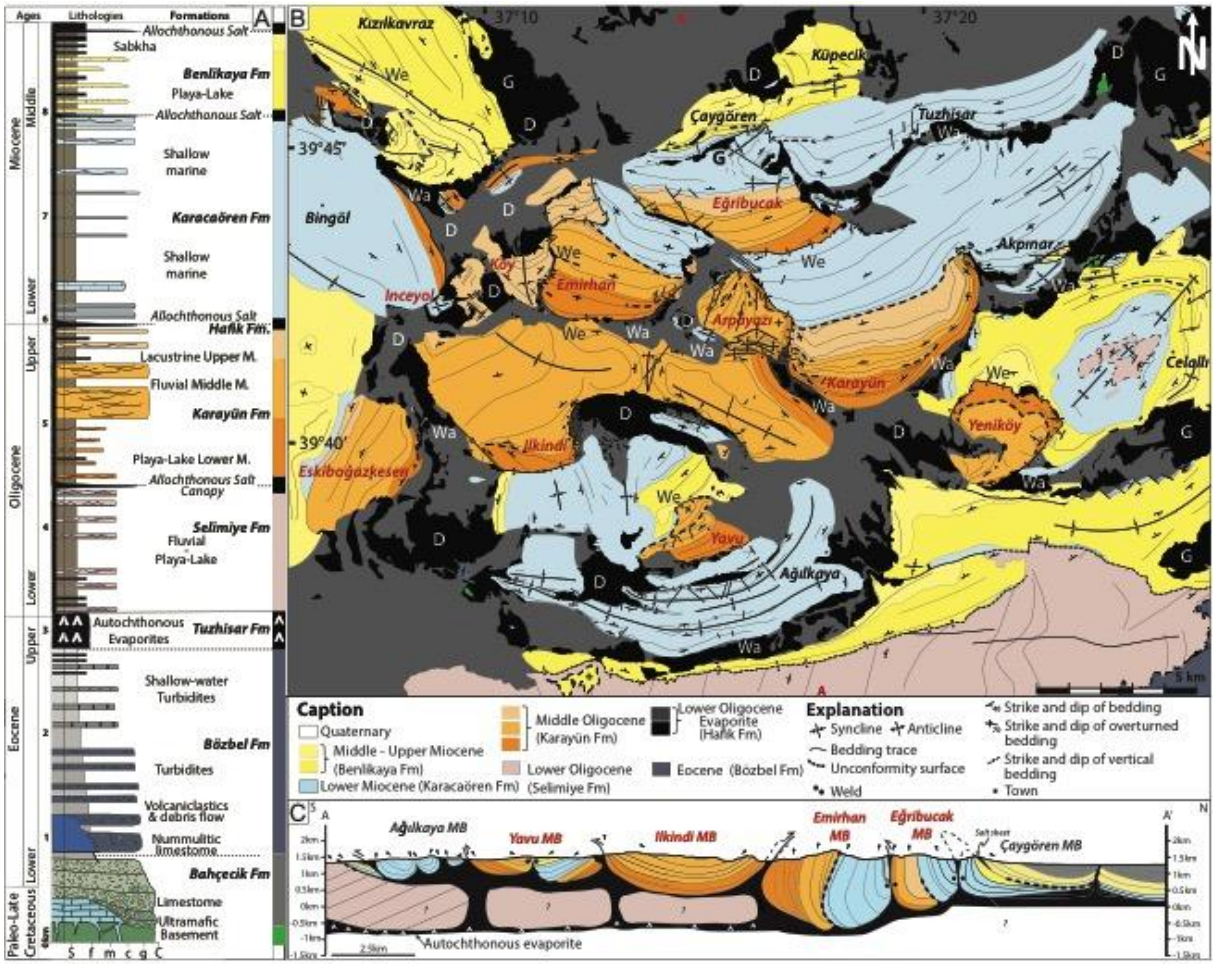
A
B
C
Ages
Lithologies
Formations
Miocene
Middle
Lower
Oligocene
Upper
Lower
Eocene
Upper
Lower
Paleo-Late Cretaceous
Allochthonous Salt
Sabkha
Benlikaya Fm
Playa-Lake
Allochthonous Salt
Shallow marine
Karacaören Fm
Shallow marine
Allochthonous Salt
Hafik Fm.
Lacustrine Upper M.
Fluvial Middle M.
Karayün Fm
Playa-Lake Lower M.
Allochthonous Salt Canopy
Selimiye Fm
Fluvial
Playa-Lake
Autochthonous Evaporites
Tuzhisar Fm
Shallow-water Turbidites
Bözbel Fm
Turbidites
Volcaniclastics & debris flow
Nummulitic limestone
Bahçecik Fm
Limestone
Ultramafic Basement
S f m c g C
Kızılkavraz
37°10
37°20
Küpecik
Çaygören
Tuzhisar
39°45'
Bingöl
Eğribucak
Akpınar
Köy
Emirhan
İnceyol
Arpayazı
Karayün
Çelallı
Yeniköy
39°40'
İlkindi
Eskiboğazkesen
Yavu
Ağılkaya
5 km
Caption
Quaternary
Middle - Upper Miocene (Benlikaya Fm)
Lower Miocene (Karacaören Fm)
Middle Oligocene (Karayün Fm)
Lower Oligocene (Selimiye Fm)
Lower Oligocene Evaporite (Hafik Fm)
Eocene (Bözbel Fm)
Explanation
Syncline
Anticline
Bedding trace
Unconformity surface
Weld
Strike and dip of bedding
Strike and dip of overturned bedding
Strike and dip of vertical bedding
Town
Ağılkaya MB
Yavu MB
İlkindi MB
Emirhan MB
Eğribucak MB
Çaygören MB
Autochthonous evaporite
2.5km